The Importance of Subsurface Productivity in the Pacific Arctic Gateway as Revealed by High-resolution Biogeochemical Surveys

L. W. Juranek[1], B. Hales[1], N. L. Beaird[1], M. Goñi[1], E. Shroyer[1], J. G. Allen[2], A. E. White[2]

[1] College of Earth, Ocean and Atmospheric Sciences, Oregon State University, Corvallis, OR USA

[2] Department of Oceanography, Daniel K. Inouye Center for Microbial Oceanography: Research and Education (C-MORE), University of Hawai'i at Manoa, Honolulu, HI 96822, USA

Corresponding author: Lauren Juranek (`laurie.juranek@oregonstate.edu`)

Key Points:

- We conducted novel high-resolution surveys of the Chukchi shelf in the Pacific Arctic to reveal whole water column biogeochemical structure
- We resolved vertical layering of subsurface features that imply significant subsurface biological productivity
- We explain spatial patterns in subsurface features in the context of stratification, turbulence, light, and seasonal water mass formation

ABSTRACT

Following sea-ice retreat, surface waters of Arctic marginal seas become nutrient-limited and subsurface chlorophyll maxima (SCM) develop below the pycnocline where nutrients and light conditions are favorable. The productivity associated with these "hidden" features has traditionally not been well constrained. Here, we use a unique combination of high-resolution biogeochemical and physical observations collected on the Chukchi shelf in 2017 to constrain the fine-scale structure of nutrients, O_2, particles, SCM, and turbulence. We find large O_2 excess at mid-depth, identified by positive saturation (O_2) maxima of 15-20% that unambiguously indicate significant subsurface production. The O_2 maxima were situated immediately beneath the pycnocline and coincided with a complete depletion of inorganic nitrogen ($[NO_3^-] + [NH_4^+]$). The complete nutrient drawdown and O_2 excess from this horizon is consistent with subsurface production that amounts to 1/3 to ½ the total regional primary production. Nitracline depths aligned with both the base of the mid-depth O_2 maxima and with SCM depths, suggesting this horizon represents a compensation point for balanced growth and loss. Furthermore, SCM were also associated with turbulence minima and sat just above a high turbidity bottom layer where light attenuation increased significantly due to high particle loads. Spatially, the largest O_2 maxima were associated with high nutrient winter-origin water masses, under a shallower pycnocline associated with seasonal melt. These data implicate short-term and

long-term control of SCM and associated productivity by stratification, turbulence, light, and seasonal water mass formation, with corresponding potential for climate-related sensitivities.

Plain Language Summary

Coastal seas in the Arctic are experiencing large changes as the region experiences warming. Some of these changes may be occurring beneath the surface, where we have fewer observations. Here, we used a unique sampling approach that allowed us to collect more observations throughout the whole water column than are typically possible, giving us a clearer picture of distinct layers at different depths. We interpreted observations of dissolved oxygen, chlorophyll, nutrients, light, and small-scale physical motions known as turbulence in different ocean layers to indicate biological growth occurring beneath the surface represents an important fraction of the total productivity for the region. We also find that we can explain vertical and spatial patterns in our data based on our understanding of how light and nutrients influence phytoplankton growth, and how ocean circulation impacts the availability of light and nutrients in the water column. These results contribute to an improved understanding of Arctic primary productivity and potential sensitivities to future change, and argue for the need to use observational tools that see below the ocean's surface to track this change.

1. Introduction

The immense and shallow continental shelves and associated marginal seas that constitute roughly half of the Arctic Ocean on an area basis host some of the most biologically productive regions in the global oceans (e.g., Hill et al., 2013; Sakshaug, 2004). Yet, in contrast to other highly productive coastal regions, these shelves spend a large proportion of the ice-free, sunlit growing season with primary production limited by a depletion of nutrients in the surface layer (Codispoti et al., 2013; Tremblay et al., 2015; Tremblay & Gagnon, 2009). The seasonal timing of these disparate conditions -- high nutrient, high chlorophyll as ice retreats and low nutrient, low chlorophyll conditions as open water dominates -- is both a hallmark feature of Arctic marginal seas and one that makes their ecological functioning sensitive to climate-induced changes (Wassmann et al., 2021; Wassmann & Reigstad, 2011). As Arctic surface temperatures warm at a pace nearly four times the global average (Rantanen et al., 2022), the profound changes in the extent and duration of the seasonal ice zone (Barnhart et al., 2016; Stammerjohn et al., 2012; Stroeve & Notz, 2018) have the ability to impact stratification and nutrient availability via control on the seasonal evolution of upper ocean forcing and stratification. These physical system changes in turn have attendant consequences for spatial and temporal patterns of productivity and trophic transfer through Arctic ecosystems. Our ability to track and understand the mechanisms by which these changes alter carbon, nutrient, and energy flows through Arctic systems is of paramount importance for improving predictions concerning how future change will manifest.

Ongoing remote sensing analyses of the Arctic Ocean and marginal seas have indicated significant, progressive increases in ocean color accompanying sea ice decline and expansion of open water, with likely contributions from both increased light and nutrient availability (Arrigo & van Dijken, 2011, 2015; Lewis et al., 2020; Pabi et al., 2008). With a longer growing season, thinner ice, and more open water area, phytoplankton productivity potential has increased. However, the largely oligotrophic status of the majority of the Arctic Ocean in summer tempers this potential (Hill et al., 2018; Juranek, 2022; Tremblay et al., 2015). In addition, regional differences in stratification, circulation, and bathymetry all help to drive regionally different responses to climate-driven change that can manifest as opposing productivity trends. For example, in the Beaufort Sea deep basin, stratification has increased from warming and freshening and the nitracline has deepened, which has likely reduced surface phytoplankton productivity (Carmack et al., 2006; Carmack et al., 2016; Carmack, 2007; McLaughlin & Carmack, 2010). However, on the continental shelf in the nearby Chukchi Sea, a shallower nitracline and prolonged open water season has allowed fall storms to mix nutrients upward and relieve surface nutrient limitation, which facilitates fall phytoplankton blooms (Ardyna et al., 2014; Ardyna & Arrigo, 2020; Juranek et al., 2019). Indeed, recent observational and modeling studies have indicated a reduced impact of the biological pump on air-sea CO_2 exchange in the Beaufort Sea and an enhanced uptake in the Chukchi Sea (Cai et al., 2010; Else et al., 2013; Ouyang et al., 2020; Tu et al., 2021), indicating that productivity changes will have important and complex feedbacks on atmospheric CO_2 and climate.

Surface productivity tracked by ocean color is only part of the equation. Though the massive phytoplankton blooms associated with thinning ice and ice retreat in nutrient-rich marginal seas in spring are a fundamental aspect of Arctic ecosystem functioning (Ardyna & Arrigo, 2020; Arrigo et al., 2012), so too are the low surface nutrient and chlorophyll conditions that typify the majority of the open water season (nominally July to October; Hill et al., 2013). During this post-bloom summer growing season much of the biogeochemical potential sits well below the surface, where a nitracline situated below the pycnocline separates nutrient-replete and nutrient-deplete waters (Codispoti et al., 2005, 2013; Tremblay & Gagnon, 2009). Subsurface chlorophyll maxima (SCM) develop throughout the majority of the Arctic Ocean in regions where surface nutrients are depleted and strong stratification prevents nutrient replenishment, including the Chukchi, Barents, Beaufort, Canadian Archipelago, Baffin Bay, and the East Siberian Shelf (e.g., Ardyna et al., 2013; Brown et al., 2015; Hill et al., 2018; Martin et al., 2010). These SCM are predictable features of stable, stratified oceans where nitraclines occur at a depth with sufficient light (Cullen, 2015) such that at the community scale, growth can be maintained in excess of respiration and grazing losses (i.e., above the compensation depth, Sverdrup, 1953). Because these features sit well below the first optical depth and are typically invisible to the passive visible spectrum sensors commonly used to retrieve chlorophyll from space, their impact is not explicitly included in estimates of

Arctic productivity increases from ocean color. The limited observational capacity means we have little information regarding how productivity occurring at SCM may be responding to climate-driven changes.

Furthermore, there is still considerable debate regarding the relative importance of SCM toward annual integrated productivity. This debate is clearly illustrated by two independent studies that used the same historical chlorophyll and productivity data set (ARCSS-PP, Matrai et al., 2013) to evaluate the potential importance of remote sensing underestimation of productivity associated with SCM: one study estimated annual Arctic Ocean productivity to be minimally underestimated (<10%; Arrigo & van Dijken, 2011) while another found underestimations to be significant (40-75%, Hill et al., 2013). Clearly, the methods and assumptions inherent in either study affect outcomes. In the former, calculation of a mean chlorophyll/productivity profile in large Arctic Ocean sectors that contained both shelf and deep basin locations likely led to a mean profile that minimized overall SCM contributions. SCM occur at different depths and have markedly different seasonality in these different regimes (e.g., in the Chukchi Sea ~20 to 30 m on shelf and 30-40 m in the Canada Basin) (Brown et al., 2015). In the analysis of Hill et al. (2013), the upper end estimate (75%) was derived from a comparison of total euphotic zone productivity versus that integrated only in the first optical depth or MLD; because this approach assumes remote sensing algorithms miss the entire contribution of lower layer productivity, whereas in reality they miss a fraction of it, this estimate is likely too high (Brown et al., 2015). However, the 40% estimate in the Hill et al. (2013) analysis was based on application of a productivity-light (P vs. E) relationship to regional profiles, with attention to seasonal stratification setting (ice-covered, partial ice-cover, open water). The seasonal/regional analysis served to highlight important differences in subsurface productivity based on timing and location: in particular, regions situated at entry and exit points with respect to circulation to/from sub-Arctic seas (referred to as inflow and outflow shelves, respectively; Carmack & Wassmann, 2006) were identified as locations where SCM productivity may be particularly significant during the partially ice-covered and open water seasons.

Here, we provide new observational constraint on the significance of subsurface production in the Chukchi Sea, an important Arctic inflow shelf and one of the most biologically productive ecosystems in the global oceans (Hill et al., 2018). Using a unique, high-resolution pumped profiling instrument we collected sections of hydrography, nutrients, dissolved oxygen (O_2), chlorophyll fluorescence, photosynthetically active radiation (PAR), beam attenuation, and turbulence data on several 40 km to 100 km surveys of the NE Chukchi shelf in 2017. These novel data reveal a layered biogeochemical structure, with extensive accumulation of dissolved O_2 and a depletion of nutrients from mid-depth waters, particularly those associated with high nutrient remnant winter water masses. The data also allow evaluation of SCM relative to finely (vertically) resolved gradients of nutrients and turbulence. We discuss the short-term and long-term processes influencing the accumulation of O_2, its association with observed SCM, and the potential importance for Arctic ecosystem and biogeochemical function

given ongoing physical system change.

1. **Observational Data and Methods**

In August 2017 we conducted high resolution surveys of the NE Chukchi shelf (**Figure 1**) on the *R/V Sikuliaq* (cruise ID SKQ201712S) using a towed vehicle with water pumping capabilities (i.e., the "SuperSucker"; (Hales et al., 2005, 2005, 2006). This platform enabled high-resolution surveys of common sensor-based observations coupled with novel, microstructure-based turbulence measurements and high-resolution inorganic nutrient and carbon concentrations via fast-response automated analysis of the pumped flow. To augment these data and further explore trends, we use CTD transect and bottle data from 2017 (SKQ201712S) as well as additional cruises in the same study area in other years, including the *R/V Ronald H. Brown* in August 2015 (RB1505) and *R/V Sikuliaq* in September 2016 (SKQ201612S) (**Figure 1**).

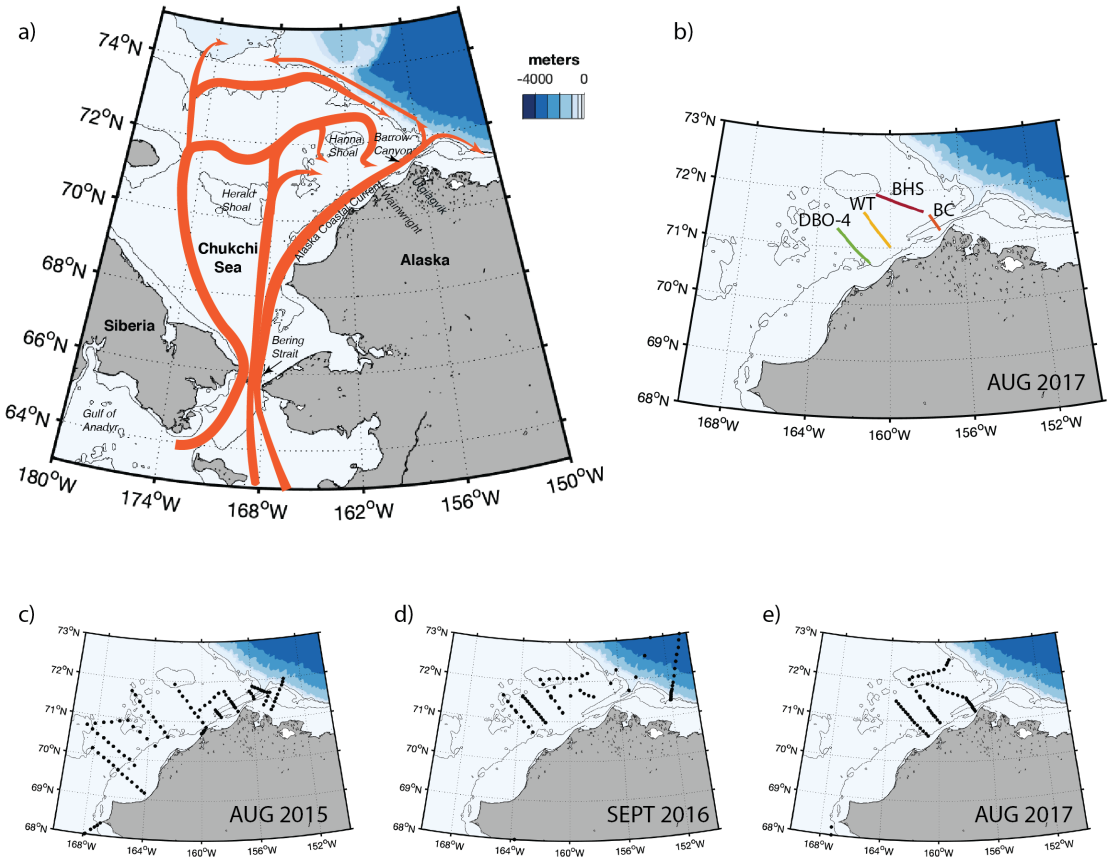

Figure 1: (a) Area map showing generalized circulation of Pacific origin water

in the study region after Pickart et al., (2019), as well as place names referred to in the text; (b) location of SuperSucker transects in the NE Chukchi Sea; (c-e) location of CTD stations for RB1505, SKQ201612S, and SKQ201712S cruises, respectively.

2.1 SuperSucker

SuperSucker surveys were conducted along historically occupied hydrographic sampling lines in the NE Chukchi, including some transects of the Distributed Biological Observatory (DBO, Grebmeier et al., 2015, 2019). These survey lines were, from east to west: a transect across Barrow Canyon (here referred to as the Barrow Canyon transect, BC), a transect between the northern edge of Barrow Canyon and Hanna Shoal (BHS), a transect offshore of the village of Wainwright (WT), and a historical transect slightly to the west of the WT transect known as DBO-4 (**Figure 1b**). The WT and BC transects were reoccupied with the SuperSucker over the course of the cruise for a total of 6 SuperSucker surveys.

Some of the SuperSucker transects occupied in 2017 were collected during or just following the influence of an upwelling event, while others reflect non-upwelling, "normal" conditions. The NE Chukchi shelf, and in particular the area near Barrow Canyon, is known to experience upwelling during periods of easterly winds; this upwelling often leads to reversal of currents in the vicinity of Barrow Canyon (**Figure 1**) and influences local hydrographic conditions significantly (c.f. Pickart et al., 2011, 2013). In mid-August 2017 (August 12^{th}-16^{th}) strong easterly winds drove an upwelling event, and the wind-induced circulation reversal caused a major redistribution of water masses in the upper water column near Barrow Canyon, as previously described by Beaird et al., (2020). Because the impact of this event on water column structure has already been described elsewhere, and because we seek to compare regional biogeochemical data collected under non-upwelling conditions, we focus on SuperSucker transects collected outside of the immediate influence of this event. These transects include the first occupation of BC (August 9^{th}-10th), BHS (August 17^{th}-18^{th}), the 2^{nd} occupation of WT (August 19th), and DBO-4 (August 13^{th}-14^{th}). Though the DBO-4 transect was occupied during the upwelling event, this section is sufficiently far west of Barrow Canyon that the influence of upwelling is limited.

The SuperSucker is an autonomously controlled sensing and sampling system that consists of a winch, sled, and submersible pump. A full sensor suite was mounted on the sled, including a SBE 911plus with dual pumped temperature/conductivity, altimeter, PAR (Biospherical Instruments QSP-200L), dissolved O_2 (SBE-43), chlorophyll fluorescence (Chl Fl, Wetlabs Wetstar), and beam attenuation (c_p, Wetlabs C-star). The submersible pump on the sled supplied water from depth to shipboard fast-response analyzers for determination of inorganic nutrient concentrations (NO_3^-, NO_2^-, NH_4^+, PO_4^{3-}, Si) as the sled profiled the water column. Horizontal and vertical resolution of profiling was user-defined, set by a combination of ship speed, bottom depth, and profiling speed; for SKQ201712S ship speed was ~1 m s^{-1} (2 kts) and vertical profiling speed was 0.2 to 0.5 m s^{-1}. This led to effective horizontal resolution of 0.2 - 0.6

km for transects shown here.

PAR profiles were calibrated against a surface PAR sensor (Biospherical Instruments QSR-2150) along a transect with known chlorophyll concentrations. Briefly, surface PAR was propagated through the air-sea interface as a function of sun zenith angle and wind speed (Mobley and Boss, 2012) and then calculated at the first optical depth following Morel et al, (2007). These values were used to derive a power law function to convert PAR voltages to scalar PAR at depth over all transects

We calibrated dissolved O_2 data by comparison to Winkler bottle O_2 data collected from the pumped flow (with SuperSucker held at fixed depth) and via comparison to a second, separately-calibrated SBE-43 O_2 sensor that was plumbed into the *R/V Sikuliaq's* science seawater system, which has a nominal intake depth of 6 m. The corrected O_2 data were used to compute the O_2 saturation (O_2) in % as follows:

$$O_2 = 100 \left(\frac{[O_2]}{[O_2]_{\text{eq}}} - 1 \right) \quad (1)$$

where $[O_2]_{\text{eq}}$ refers to the solubility equilibrium for O_2 based on co-located temperature (T) and salinity (S) assuming standard atmospheric pressure, calculated according to Garcia and Gordon, (1992).

Turbulence was derived from microstructure temperature GusT sensors (Moum, 2015) mounted on the leading edge of the SuperSucker sled. Temperature microstructure measured at 100 Hz was used to calculate the rate of dissipation of temperature variance (χ_T) and turbulent temperature diffusivity (K_T) following Moum and Nash (2009). Further details of GusT measurements and computation of K_T are described in Beaird et al. (2020).

Nutrients were measured on the pumped flow by fast-response shipboard analyzers (Hales et al., 2004). Nutrient data were calibrated using standard curves run approximately every 2 hours and phase-shifted for analytical and sampling lag times relative to in situ sensor data.

While data have been aligned to account for known phase shifts, the dynamic response time of individual sensors or analytical systems, combined with profiling speed, determine effective resolution. For dissolved O_2, the SBE-43 response time at seawater temperatures -2 to 10° C was approximately 4 s; for shipboard nutrient analysis the response time was ca. 15 s. These lagged dynamic responses act to low-pass filter observed O_2 and nutrient concentrations, and together with the vertical profiling speed, yield effective resolution of observed gradients is 1 to 3 m. After calibration and time lag adjustments, all SuperSucker sensor data, GusT-derived turbulence parameters, and inorganic nutrient concentrations were averaged into 1m vertical bins prior to plotting.

1. **CTD and bottle data**

We supplement our analysis with sensor and bottle data collected using standard

CTD and rosette sampling in August 2015 on RB1505, in September 2016 on SKQ201612S, and August 2017 on SKQ201712S (**Figure 1**). On each cruise, a SBE 911plus equipped with dual pumped conductivity/temperature, dissolved O_2, PAR, and Chl Fl was used to collect profile data for transects across the NE Chukchi shelf. Data for RB1505 were processed and corrected by the NOAA EcoFOCI group. Data collected during SKQ201612S and SKQ201712S were processed according to best practices outlined by the manufacturer (SeaBird Instruments) and binned into 1 db intervals. SBE-43 O_2 data were corrected for sensor lags relative to temperature and conductivity and were compared to bottle O_2 data collected from the upcast and analyzed via Winkler titration. CTD data are used here to demonstrate that features observed in SuperSucker transects are typical of late summer conditions.

1. **Results**

3.1 Layered hydrographic and biogeochemical features in 2017 SuperSucker surveys

SuperSucker transects indicate strong water column stratification contributed to a layered vertical structuring of biogeochemical tracers throughout the study area in 2017 (**Figures 2 & 3**). A pycnocline situated between 15 m and 25 m (identified by the water column maximum of the Brunt-Väisälä buoyancy frequency, $N^2 = \frac{-g}{\sigma_\theta}\frac{d\sigma_\theta}{\mathrm{dz}}$, where g is gravitational acceleration, σ_θ is potential density, and z is depth) isolated subsurface waters from the surface mixed layer, with surface waters depleted in dissolved inorganic N (DIN, approximated here as NO_3^- + NH_4^+). Near-bottom waters were nutrient-replete, with [NO_3^-] generally ranging from 2 to 12 µM and [NH_4^+] ranging from 0 to 6 µM. Dissolved O_2 saturations were slightly positive but near equilibrium (O_2 = 0%) in surface waters, while below the pycnocline, at mid-water column depths, high O_2 supersaturations were observed (O_2 up to 20%). The O_2 magnitude and layer thickness varied spatially: largest signals were generally observed in areas of the shelf directly overlying bottom waters with high concentrations of nitrate and ammonium. These high nutrient bottom waters were generally found in eastern transects (BHS, BC, **Figure 2**), while lower nutrient bottom waters were found in transects on the western side of the study area (WT, DBO-4, **Figure 3**). Bottom water O_2 were undersaturated, consistent with a respiration-dominated regime and the absence of ventilation. The degree of undersaturation in bottom waters also varied spatially, with most negative O_2 (approaching -30%) occurring in the easternmost transects (BHS, BC) where the highest bottom water [NO_3^-] and [NH_4^+] were observed, and lower O_2 (-20%) in the bottom waters of western transects (WT, DBO-4).

Sensor-based proxies for phytoplankton biomass and particles on SuperSucker transects also indicated distinct water column layers in these properties. Chlorophyll fluorescence (Chl Fl) was generally low in surface and near-bottom waters, but was often elevated in mid-depth waters, consistent with SCM commonly observed in this region (Brown et al., 2015; Hill et al., 2013; Martini et al., 2016;

Weingartner et al., 2017). The Chl Fl signals were always coincident with the nitracline in a given transect but were spatially patchy, with patterns that did not seem to be as strongly associated with bottom water nutrient concentrations as O_2 (**Figures 2 & 3**). SCM were 15-25 m deeper than the pycnocline in eastern transects (BC, BHS) and closer to the pycnocline in western transects (WT, DBO-4) (**Figures 4 & 5**). This spatial pattern in SCM positioning was similar to that previously observed by Martini et al. (2016), who observed a northeast/southwest difference which they connected to surface sea ice meltwater presence or absence. We further explore spatial patterns of the SCM and pycnocline in relation to water masses below.

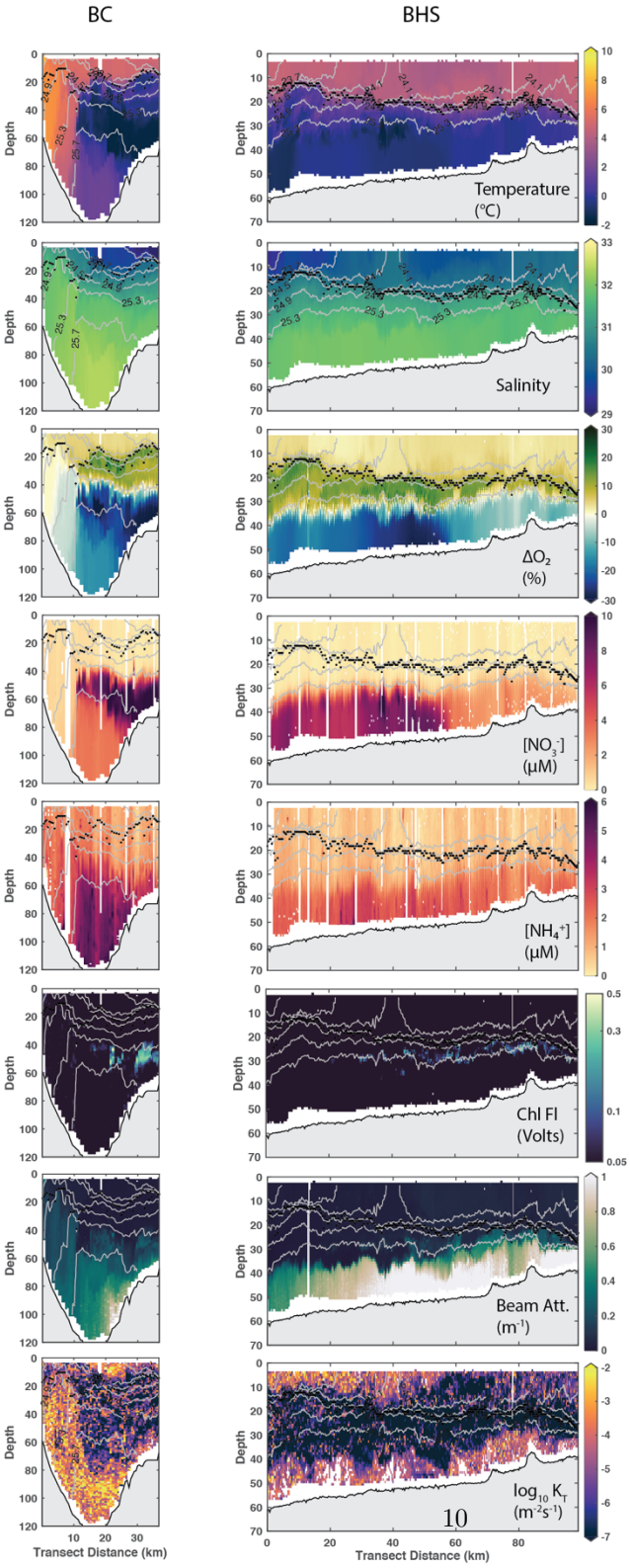
BC
BHS
Depth
Temperature (°C)
Salinity
ΔO2 (%)
[NO3-] (μM)
[NH4+] (μM)
Chl Fl (Volts)
Beam Att. (m-1)
log10 KT (m-2s-1)
Transect Distance (km)
Transect Distance (km)

Figure 2: Biogeochemical data collected by the SuperSucker on eastern study area surveys. Thin grey lines are density contours. Stippled black line is the pycnocline as defined by the water column N^2 maximum. Left hand side of each panel is the shoreward edge of transect. Note the different vertical scales for BC and BHS transects.

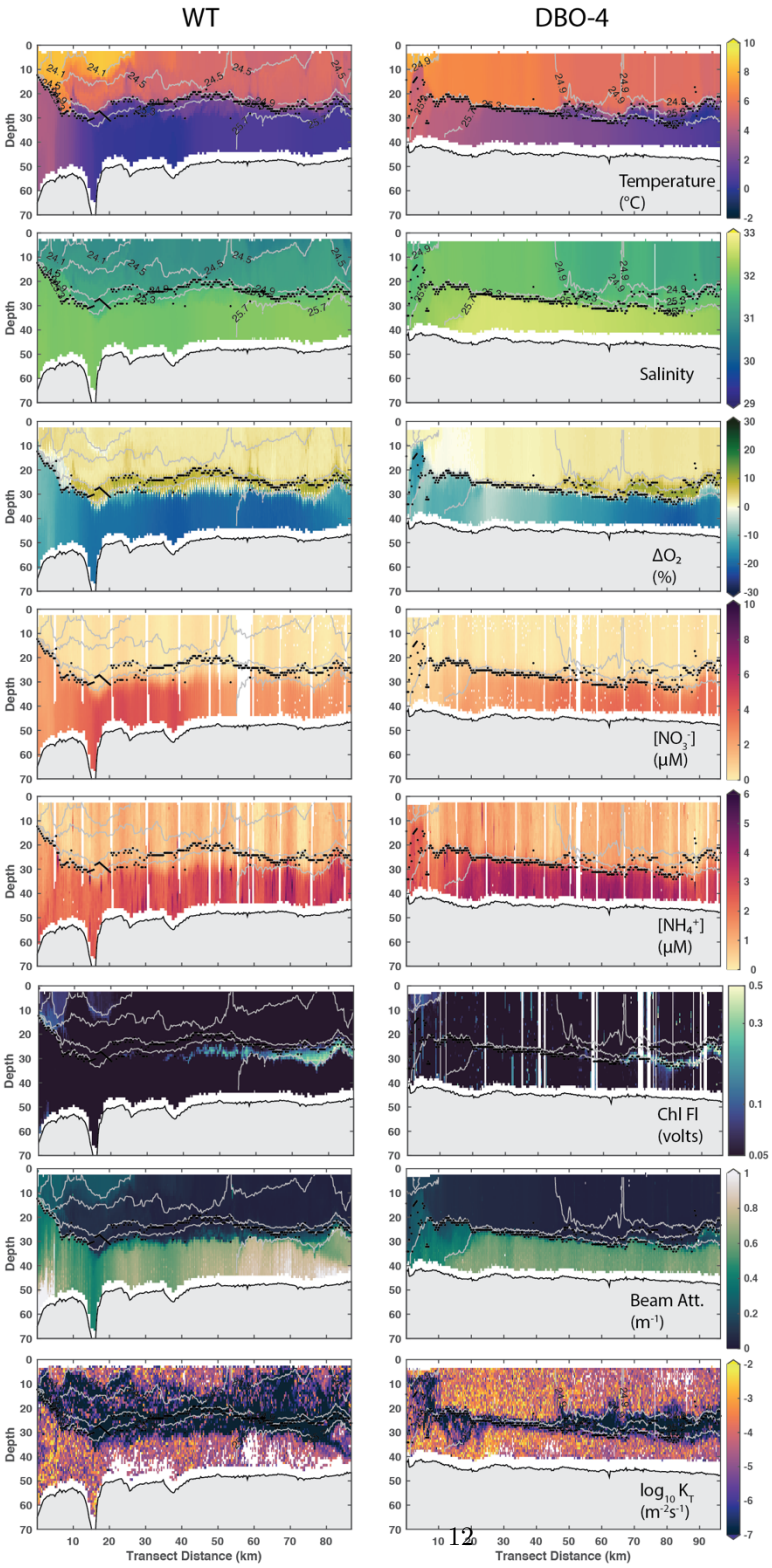
WT
DBO-4
Depth
Temperature (°C)
Salinity
ΔO2 (%)
[NO3] (µM)
[NH4+] (µM)
Chl Fl (volts)
Beam Att. (m-1)
log10 KT (m-2s-1)
Transect Distance (km)
Transect Distance (km)

Figure 3: Biogeochemical data collected by the SuperSucker on western study area surveys. Thin grey

lines are density contours. Stippled black line is the pycnocline as defined by the water column N^2 maximum. Left hand side of each panel is the shoreward edge of transect.

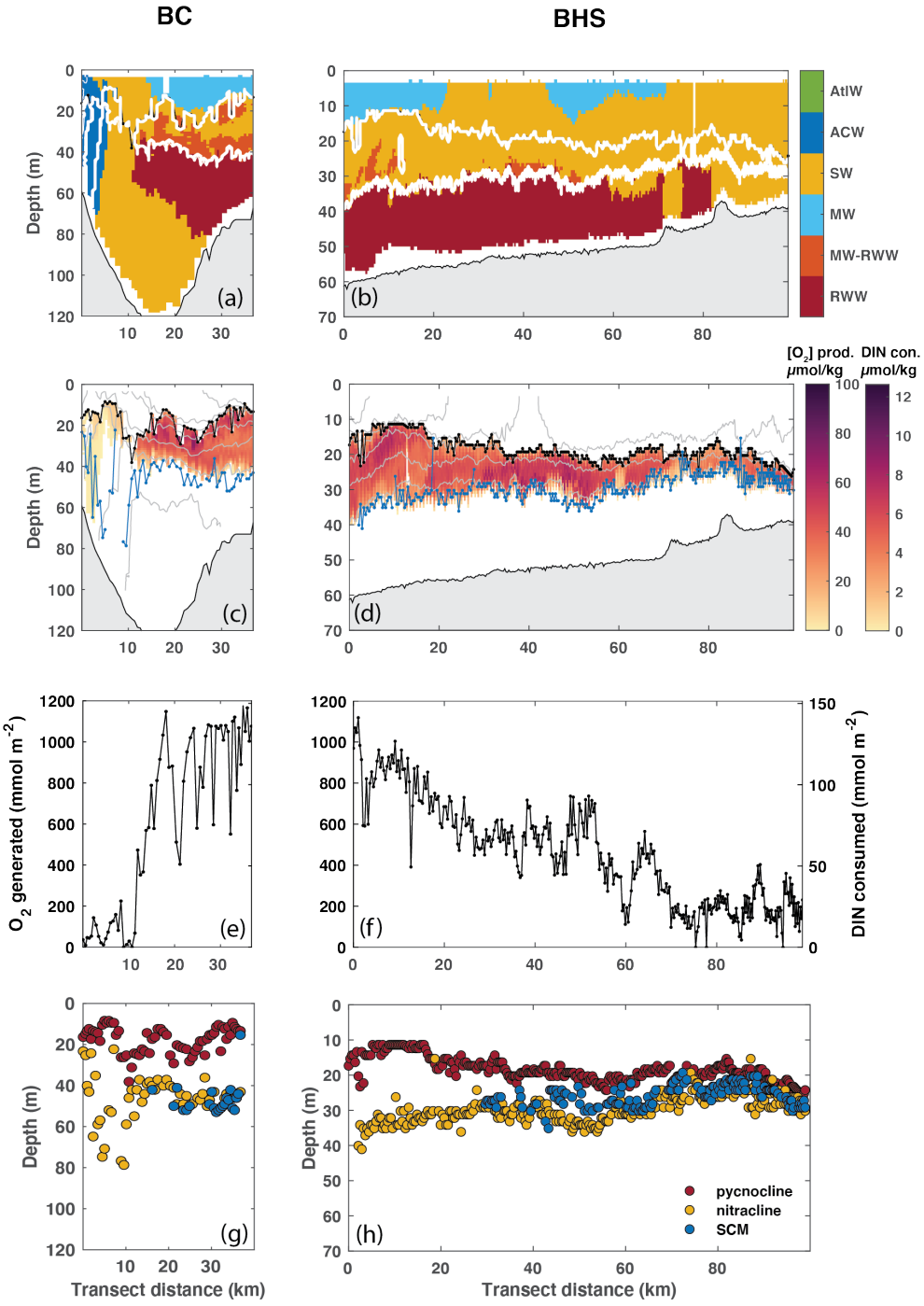

Figure 4: (a,b) Water mass classification for eastern surveys; white outline

indicates position of the O_2

maxima as defined by the region under the pyncocline with O_2 >0; (c,d)) calculated O2 excess (and

implied N consumption from stoichiometric conversion) in the subsurface O2 maxima, shown with

pycnocline (black line, defined as the water column maximum of the buoyancy frequency N^2) and

nitracline (blue line, defined as the maximum vertical DIN gradient). (e,f) calculated integrated inventory

of produced O2 and implied N consumption; (g,h) comparison of pycnocline, nitracline, and SCM depths

for each transect. The SCM was defined as the water column maximum Chl Fl gradient, and only shown

when above the noise floor of sensor measurement and when location was below the pycnocline.

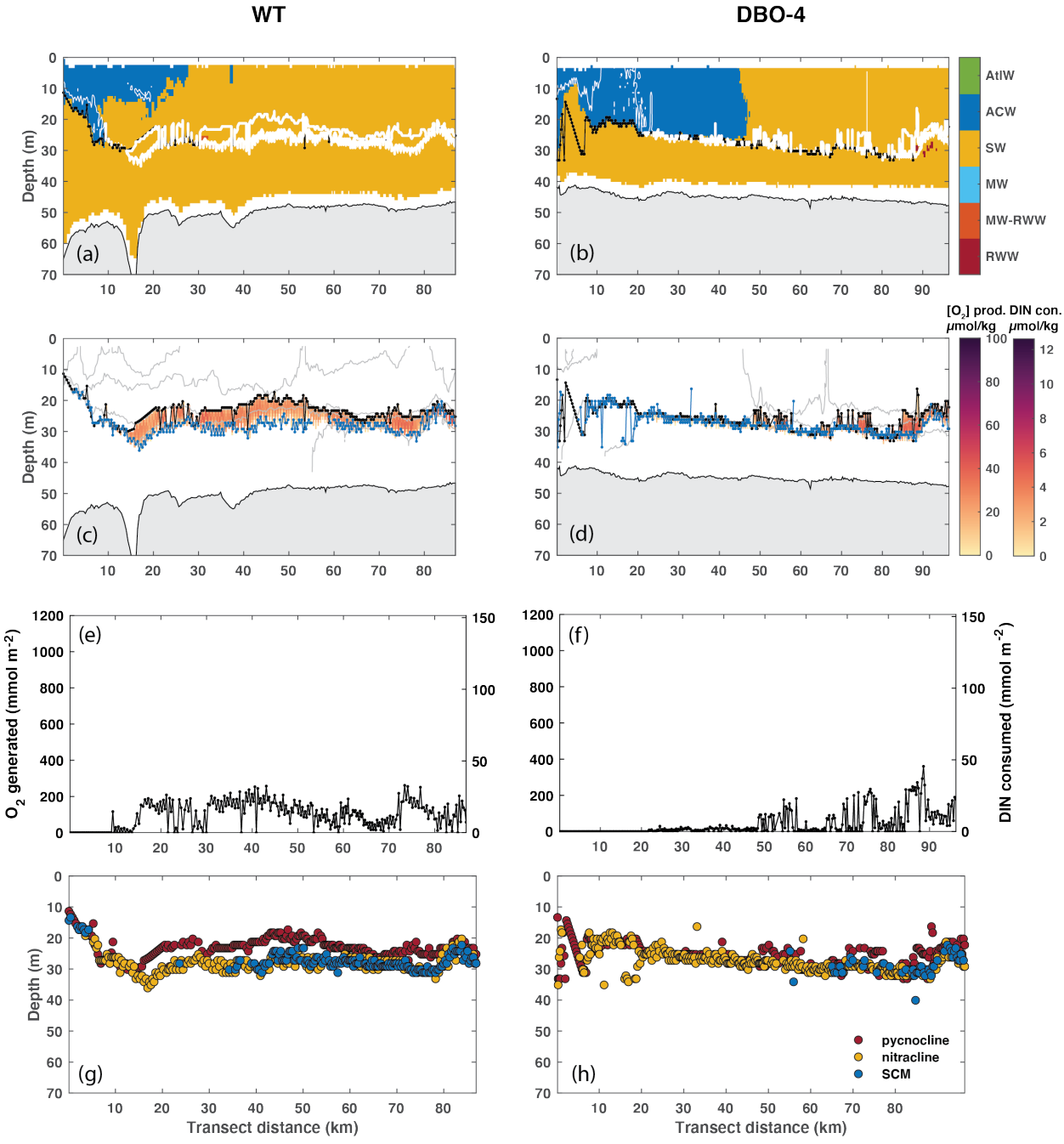

Figure 5: Same as in Figure 4, but for western transects.

The elevated Chl Fl at mid-depth should not presumed to scale linearly with

phytoplankton biomass or even chlorophyll concentration, since the relationship between Chl Fl varies regionally with community composition and nutritional status, and increased cellular chlorophyll concentrations at low light (photoadaptation) will alter biomass to chlorophyll ratios (Cullen, 2015; Fennel & Boss, 2003; Letelier et al., 2004). However, discrete samples from surface, mid-depth, and bottom water sampling previously reported by Goñi et al. (2021) indicated enhancements of chlorophyll pigment concentration and particulate organic carbon at mid-depth compared to surface waters, albeit smaller than those indicated from Chl Fl. While CTD Chl Fl indicated a nominal 6-fold increase between surface and mid-depth waters on average, there was a 2.5-fold increase of measured pigment concentration (0.78 ± 0.51 mg m^{-3} vs. 1.97 ± 0.88 mg m^{-3} in surface and mid-depth, respectively) and a 1.5-fold increase in particulate organic carbon (7.60 ± 6.07 mmol m^{-3} vs. 10.71 ± 6.88 mmol m^{-3} in surface and mid-depth, respectively), with the latter not distinguishing between phytoplankton or detrital carbon (Goñi et al., 2021). Optical beam attenuation (c_p, m^{-1}), a proxy for particle concentration, indicated little attenuation in surface waters and much higher attenuation in bottom waters (>0.5 m^{-1}), with intermediate attenuation values within SCM (**Figures 2 & 3**), suggesting highest particle loads in the bottom layer and moderate enhancements at SCM. Characterization of discrete samples indicated that particles in bottom waters were detrital whereas those in the mid-water column within SCM were more recently produced organic matter (higher chl to pheophytin pigment ratios, Goñi et al., 2021).

In order to better understand potential mechanisms driving spatial variance in O_2, Chl Fl, and other biogeochemical data, we classified the water column with respect to important regional water masses by their temperature (T) and salinity (S) properties. We used water mass classifications slightly modified after Pickart et al. (2019) as they are specific for late summer conditions in our study region (see **Table 1** for water mass T-S boundaries). Because these water masses are formed at different times and locations and are subject to different physical and biological modifications, this water mass partitioning can be used to understand processes influencing observed biogeochemical distributions. Remnant winter water (RWW) is, as the name implies, a cold, moderate salinity (i.e., T<0°C; S between 31.5 and 33.6) residual of water formed in winter in the northern Bering Sea and Chukchi Sea (Pacini et al., 2019; Pickart et al., 2016). This water mass has been associated with very high nutrient concentrations resulting from the breakdown of water column stratification in winter as well as respiration of organic matter during winter and early spring (Lowry et al., 2015; Mordy et al., 2020; Pacini et al., 2019). Because of a shelf residence time of 4-6 months (Shroyer & Pickart, 2018; Woodgate & Peralta-Ferriz, 2021) the majority of RWW is flushed off the shelf by late summer but pockets of it can remain along certain transit pathways (Lin et al., 2019), as discussed in more detail in section 4.4. Summer water (SW) is a warmer water mass (T between 0°C and 6°C) formed after ice retreat by modifications due to heat gain, mixing, and freshening (Gong & Pickart, 2016). SW is distinguished from warmer,

low salinity Alaska Coastal Water (ACW) which is typically found within the nearshore Alaska Coastal Current (**Figure 1**) in summer and early fall (Lin et al., 2019; Pickart et al., 2019; Shroyer & Pickart, 2018). ACW is significantly influenced by regional terrestrial freshwater inputs and tends to be DIN-poor (Coachman et al., 1975; Walsh et al., 1989). Low salinity Meltwater (MW) (S<30) arises from seasonal sea ice melt and is primarily encountered at the surface. Finally, Atlantic water (AW) is a saline (S>33.6), nutrient-rich water mass which resides at depth in the Arctic Basin but can also be encountered intermittently on the Chukchi shelf during wind-forced upwelling events (e.g., Pickart et al., 2013, 2019).

Table 1: Water mass criteria. Temperature (T) and Salinity (S) thresholds are the same as those used by Pickart et al. (2019) for late summer in this study region with the exception of the temperature threshold delineating the boundary between SW and ACW. The overall warmer conditions in our study region in 2017 meant that SW had a broader temperature range.

Water mass	Temperature	Salinity
Remnant Winter Water (RWW)	T<0	< S <33.6
Meltwater-Modified RWW (MW-RWW)	T<0	S<31.5
Meltwater (MW)	T>0	S<30
Summer Water (SW)	<T<6	<S<33.6
	T>6	32<S<33.6
Alaska Coastal Water (ACW)	T>6	<S<32
Atlantic Water (AtlW)		S<33.6

Clear contrasts were evident between eastern and western transects with respect to water mass presence (**Figures 4 & 5**). In eastern transects (BHS, BC) water column profiles were typically comprised of at least 3 water mass layers, with RWW typically encountered in near-bottom waters, SW or a slightly fresher variant of RWW (referred to as meltwater-influenced RWW) in mid-depth waters and MW or SW at the surface. A plume of ACW was only encountered on the nearshore end of the BC transect, as expected. In western transects (WT, DBO-4) ACW was again encountered nearshore but the offshore water column was entirely comprised of SW.

Differences were also apparent in patterns of pycnocline, SCM, and nitracline depths amongst the eastern/western water mass regimes. The pycnocline (identified by max N^2) was deeper (generally >20 m) in regions where SW was present at the surface and shallower (<20 m) when MW was present at the surface (**Figures 4 & 5**). SCM and nitracline depths (determined by max vertical gradients in Chl Fl and DIN, respectively) were tightly coupled for all

transects, but were generally much closer to the pycnocline in western transects (WT, DBO-4) where the pycnocline was deeper. The gap between the pycnocline and nitracline aligned nearly perfectly with the mid-depth O_2 maxima. Hence, the largest O_2 maxima occurred where the vertical gap between the pycnocline and the nitracline was largest, i.e., profiles characterized by MW at the surface (**Figure 4 & 5**). The base of the mid-depth O_2 maxima (defined as the depth where O_2=0%) was coincident with nitracline and SCM depths (**Figures 4 & 5**), indicating that these features are situated at a horizon where a net community photosynthetic regime above gives way to a net community respiratory regime below, also referred to as the compensation depth (Sverdrup, 1953).

We further examined these spatial contrasts by computing average profiles of density, stratification (N^2), turbulent diffusivity calculated from microstructure (K_T), O_2, Chl Fl, DIN (approximated as $[NO_3^-] + [NH_4^+]$), and turbulent DIN flux (i.e.,$< K_T \frac{d\ (DIN)}{\mathrm{dz}} >$, mmol m^{-2} d^{-1}) from each 2017 transect according to the water mass present at the surface (**Figure 6**). These profiles illustrate substantial variability from profile to profile, particularly for stratification, turbulence, and Chl Fl. However, composite average profiles indicate clear commonalities and differences in features of the hydrographic regimes. These profiles reinforce much of the generalized conclusions regarding pycnocline, SCM, O_2 and nitracline features seen in the transects: the pycnocline is shallower, and the distance between the pycnocline and nitracline/SCM larger for profiles where MW is present at the surface compared to those where SW is present. It is in this vertical gap that largest O_2 maxima sit. Turbulence tended to be highest in surface and bottom layers (i.e., O(10^{-4}) and above), with a local minimum in the vicinity of the N^2 max which, given that K_T is indirectly related to the inverse of stratification, is not surprising (**Figure 6**). Perhaps most importantly, SCM appeared to align with local minima in K_T, which suggests that low turbulence is a factor in allowing SCM to persist. For most transects the K_T minimum and SCM tended to be around 25-30 m (WT, DBO-4, BHS) but for the BC transect, the Chl Fl maximum, the nitracline, and K_T minimum were observed much deeper at ~45 m (**Figure 4, Figure 6**). Despite large differences in bottom water DIN (i.e., $[NO_3^-] + [NH_4^+]$) between eastern and western transects, the turbulent N flux from nutrient-replete bottom waters toward the mid-depth water column was remarkably similar, with values O(10^0) mmol m^{-2} d^{-1} and approaching O(10^1) (**Figure 6**). These significant nutrient fluxes were produced via a combination of moderate to high K_T occurring below the stratification maximum but still within the nitracline where DIN gradients were large.

3.2 CTD surveys from 2015-2017 confirm consistent subsurface O_2 maxima

Dissolved O_2 and Chl Fl data from CTD profiles collected from the same study region in August 2015 and September 2016 indicate consistent presence of late season subsurface O_2 maxima and association with certain water masses. We include CTD profile data from the August 2017 SKQ201712S cruise for compar-

ison.

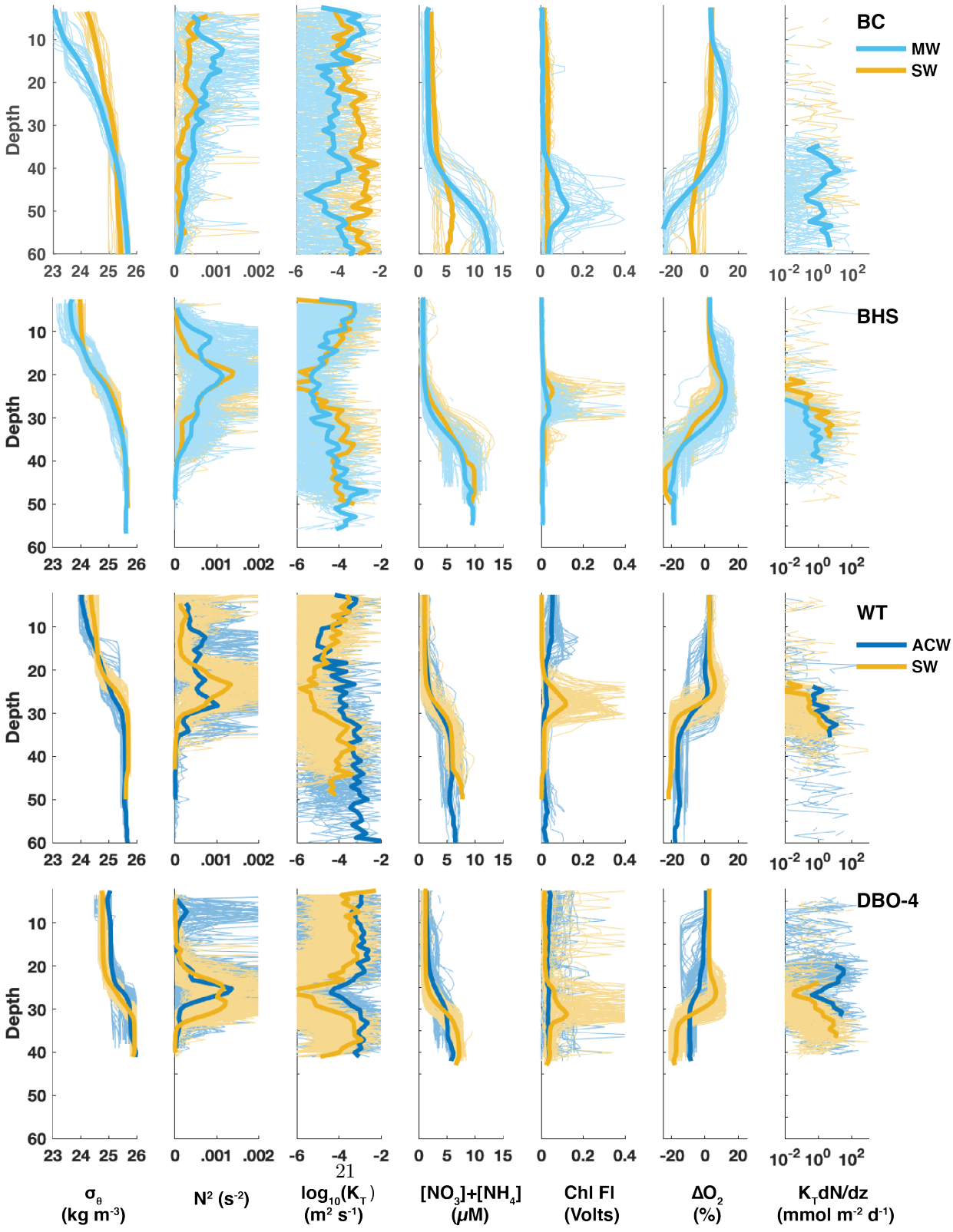
BC
MW
SW
BHS
WT
ACW
SW
DBO-4
Depth
10
20
30
40
50
60
23 24 25 26
0 .001 .002
-6 -4 -2
0 5 10 15
0 0.2 0.4
-20 0 20
10^{-2} 10^{0} 10^{2}
σ_θ (kg m^{-3})
N^2 (s^{-2})
log$_{10}$(K$_T$) (m^2 s^{-1})
[NO$_3$]+[NH$_4$] (μM)
Chl Fl (Volts)
ΔO$_2$ (%)
K$_T$dN/dz (mmol m^{-2} d^{-1})

Figure 6: Individual (thin line) and average (thick line) profiles for each transect grouped by water mass present at the surface.

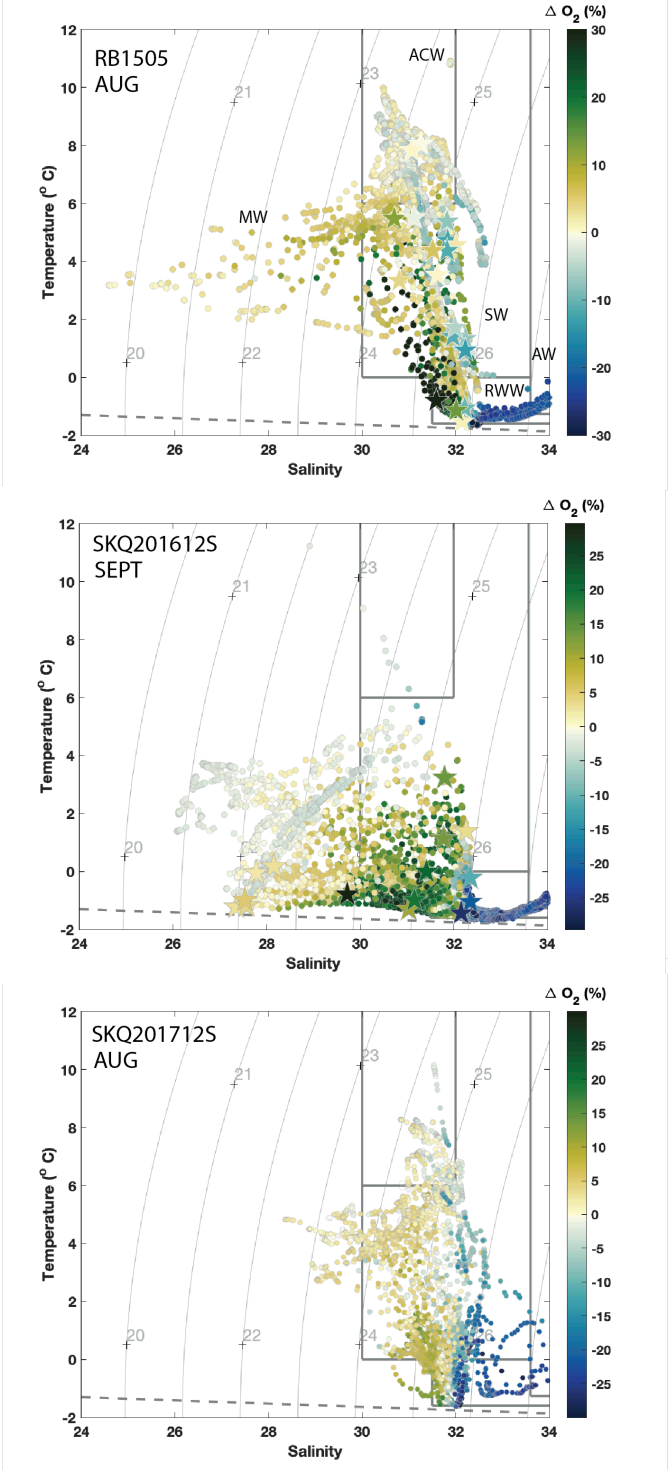
RB1505
AUG
ACW
MW
SW
AW
RWW
SKQ201612S
SEPT
SKQ201712S
AUG
Temperature (° C)
Salinity
Δ O2 (%)

Figure 7: T-S diagrams of CTD profile data from 2015-2017 cruises, colored by O_2 Also shown are

lines of constant density (thin grey curved lines) and boxes denoting water mass types. Colored stars in

top and middle panel indicate discrete O2/Ar saturation data collected on RB1505 and SKQ201612S

cruises.

The 2015-2017 cruise data reflect markedly different hydrographic conditions experienced in late summer in the Chukchi and as such are most easily compared by use of T-S diagrams with water mass designations as previously described (**Figure 7**). In general, the T-S properties of August 2015 and August 2017 were very similar, with water column temperatures ranging from near-freezing to nearly 10° C in the surface. A broader range of salinities was encountered in 2015 as compared to 2017, which is likely due to a broader sampling domain in 2015 that included several stations in the Beaufort Sea, where both high salinity AW and low salinity MW are likely to be encountered. The majority of the water column in September 2016 was considerably cooler and with much more substantial MW influence than in other years. These September 2016 conditions were heavily influenced by a large cyclone in August 2016 that resulted in dynamical loss of sea ice and hence, an increase in MW, in the study region prior to sampling (Petty et al., 2018; Yamagami et al., 2017).

Despite large interannual differences in hydrography, the CTD data paint a consistent picture of persistent, significant O_2 in late summer. In fact, CTD data suggest that O_2 maxima in 2015 and 2016 were even higher (exceeding 30%) than those observed in 2017 (**Figure 7**). Despite interannually variable conditions, the epicenter of high O_2 was consistently associated with RWW, or with the coldest, most dense classes of SW. In 2016, high O_2 was also associated with mixtures of RWW and MW occupying the mid-water column in the σ_θ 24.0 to 25.5 kg m^{-3} range.

1. **Discussion**

4.1 Mid-depth O_2 saturation indicates significant subsurface productivity

While a number of previous studies have documented and discussed aspects of the features described above (see section 4.2), our observations are the first that simultaneously resolve the fine-scale vertical and horizontal distributions of nutrients and turbulence relative to sensor-based Chl Fl, beam attenuation, and dissolved O_2 in this region. The patterns that emerge from these novel data provide new constraints on the importance of subsurface phytoplankton activity as well as the factors that may be responsible for observed variability.

Vertical distributions of dissolved O_2 and inorganic nutrients unambiguously indicate significant primary and net community production in subsurface wa-

ters. The large, positive O_2 observed at mid-depth can only be explained by an excess of photosynthetic input of O_2 relative to respiration. While abiotic processes including water mass warming in summer or bubble-induced supersaturation at the time of winter ventilation could drive some supersaturation, these processes cannot fully explain O_2 saturations on the order of 20% to 30%. For example, the maximum warming-induced supersaturation would be +10%: this assumes warming from a minimum temperature at the freezing point (-1.77°C for S=32.5) to 2°C (T observed at mid-depth in 2017). Bubble-induced supersaturations, which might have been imparted throughout the shallow water column during vigorous air-sea interaction in winter, are typically associated with supersaturations of 1-3% (Hamme et al., 2019; Stanley et al., 2009). Perhaps more importantly, bottle samples collected within O_2 maxima in 2015 and 2016 had O_2/Ar saturations that matched observed O_2 within a few percent (colored stars, **Figure 7**). The agreement between O_2 and O_2/Ar saturation indicates that positive O_2 is driven almost entirely by biological input of O_2, since warming and bubbles cause O_2 and Ar to increase similarly and hence would not drive large supersaturations in O_2/Ar.

Elemental stoichiometric relationships among O_2, particulate organic matter, and inorganic nutrients in mid-depth waters paint a consistent picture. In concentration units, the excess O_2 associated with O_2 maxima of 15 to 20% is 40 to 70 µmol kg^{-1} **(Figures 4 & 5)**, which would equate with net POC production of 30 to 50 µmol kg^{-1} (assuming a O_2:C for net production of 1.4; Laws, 1991). The expected inorganic N uptake for this POC production would be 5 to 8 µmol kg^{-1} (assuming canonical Redfield et al. (1963) C:N of 6.6, similar to C:N observed in this study by Goñi et al. 2021). The typical POC concentrations encountered in mid-depth waters were much lower ($\overline{x} \pm \sigma$ of 10.71$\pm$ 6.88 mmol m^{-3}; Goñi et al., 2021) indicating that a substantial proportion of generated particles had been exported from this mid-depth layer. Both NO_3^- and NH_4^+ were completely depleted over the mid-depth horizon with high O_2, as expected given uptake of available nutrients would be needed for formation of organic matter and O_2, and subsequent export of that material to depth would prevent remineralization at mid-depth.

Integrating the total O_2 excess at mid-depth yields water column O_2 production below the pycnocline of 800-1200 mmol m^{-2} for eastern transects overlying RWW and more modest production (100-200 mmol m^{-2}) in western transects where was RWW was absent (**Figures 4 & 5**). The implied subsurface N demand assuming a O_2:C for net production of 1.4 (Laws, 1991) and C:N of 6.6 (Redfield et al., 1963) would be 100-150 mmol m^{-2} of DIN in eastern transects and 25 mmol m^{-2} DIN in western transects (**Figures 4 & 5**). Given typical winter, pre-bloom [NO_3^-] of 10-12 µmol kg^{-1} in the Chukchi (Arrigo et al., 2017; Lowry et al., 2015; Mordy et al., 2020) this suggests that the subsurface O_2 maxima reflect on average the complete utilization of a pre-bloom nutrient inventory of 10 m thickness for eastern transects overlying RWW or, alternatively, the partial conversion of a thicker layer. The integrated O_2 excess is likely a minimum estimate since the O_2 feature is subject to losses from diffusive mix-

ing to lower O_2 waters above and below. Importantly, because the O_2 balance is controlled by the net production-respiration balance, the residual O_2 is an indicator of new production (*sensu* Dugdale & Goering, 1967) below the surface layer. In bottom waters where $O_2$was negative, DIN was elevated, with moderate values in western survey lines and values approaching 20 µmol kg^{-1} in some areas of the eastern survey lines, particularly in locations where O_2 deficits were largest. These observations are consistent with a significant proportion of bottom water nutrients being regenerated by respiration of exported POC after winter ventilation. We further explore bottom water nutrient stoichiometry and implications for seasonal nutrient replenishment in this region in a companion paper (Juranek et al., in prep).

Our unique combination of high-resolution nutrient, O_2, PAR, and beam attenuation data also yield interesting insight into controls on SCM depth. The co-location of SCM, nitracline, and the deepest extent of O_2 maxima (**Figures 4 & 5**) suggests that these features are positioned at a vertical horizon in the water column that represents a breakeven point with respect to community level respiration and photosynthesis; in effect this is a biogeochemical indicator of the compensation depth for the community (above which net production occurs, below which net respiration occurs; Sverdrup, 1953). The accumulation of O_2 excess above (but not below) and the accumulation of nutrients below (but not above) are consistent with a balance between net gain and loss at this horizon. Traditionally, this horizon is viewed to be set by the availability of light at depth (Sverdrup, 1953), although gain/loss due to turbulence and grazing might modulate this under some conditions (Cullen, 2015). One might expect that in a given geographic region with similar incident PAR and low surface chlorophyll that SCM would always occur at the same depth. However, there were systematic differences in SCM depths across transects in this region. For example, SCM and nitracline depths ranged from as shallow as 20 m at the northern end of the BHS, WT, and DBO-4 transects to as deep as 40-50m for the BC transect. The positioning of SCM and nitracline appeared to be influenced by a rapid increase in turbidity (a 'turbid-cline') associated with the bottom 10-20 m of the water column (**Figures 2 & 3**).

The relationship among PAR, turbidity, and SCM depths is made clear by looking at light attenuation evident in PAR profiles (**Figure 8**). We computed the depth-resolved attention coefficient ($\sim K_{\mathrm{PAR}}$, m^{-1}) as $\sim K_{\mathrm{PAR}} = \frac{d(lnPAR)}{\mathrm{dz}}$. The $\sim K_{\mathrm{PAR}}$ values indicate relatively constant and low attenuation in the upper water column and a rapid increase in attenuation at the onset of high turbidity. SCM depths appeared to closely track turbidicline depths and the transition to a higher light attenuation regime. This suggests that turbidity in the bottom layer is an important limit on SCM positioning as well as the depth at which there is sufficient light for net community growth to occur.

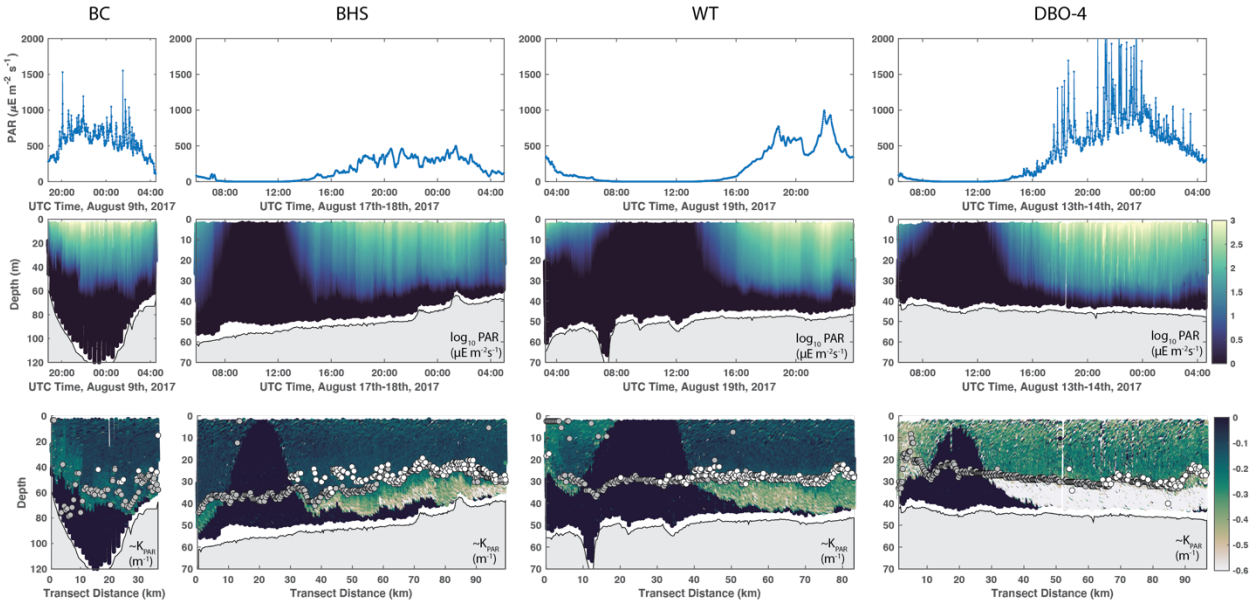

Figure 8: Relationships among PAR, turbidity, and SCM depth as seen in 2017 surveys. Top row: Surface PAR measured by a shipboard sensor during each SuperSucker transect. Middle row: In water PAR (log scale) for each SuperSucker transect. Bottom row: Diffuse attenuation of PAR as calculated by $\sim K_{\mathrm{PAR}} = \frac{d(lnPAR)}{\mathrm{dz}}$. Also shown are turbidicline depths (gray dots) as determined by a c_p threshold of >0.25, and SCM depths (white dots), as previously defined.

1. **Previous observations**

Several prior studies in our study region have identified and discussed aspects of the water column features described above and provide helpful context for further synthesis. Subsurface O_2 maxima were noted over 50 years ago in the Bering Strait and Siberian Coast regions by Codispoti & Richards, (1971), although the maxima they reported were noted to occur shallower in the water column (above 20 m) under a much shallower surface pycnocline than observed in our study, with the water column below 20 m generally undersaturated in O_2. Similar to our observations, the highest and lowest O_2 were noted to occur in near-freezing waters with S between 31 and 33 (i.e., RWW) and high O_2 was associated with significant nutrient depletion, the latter taken as evidence that the O_2 was photosynthetically generated. Later observations from the 2002 Shelf Basin Interactions program process study cruises again identified mid-depth O_2 maxima on the NE Chukchi Shelf in summer and linked their occurrence to SCM, the nitracline (Codispoti et al., 2005), and subsurface productivity maxima (Hill & Cota, 2005). Slight vertical offsets in these features were evident in their data but were not discussed. The general mid-depth co-occurrence of these features was taken by Codispoti et al. (2005) as strong evidence of sustained phytoplank-

ton production at the nitracline in summer as surface nutrient inventories and phytoplankton biomass decrease and water column light penetration increases. More recently, Lowry et al. (2015) drew a connection between presence of high-nutrient RWW, Chl Fl, and high O_2 in early season sampling (June-July) in the NE Chukchi associated with the Impacts of Climate on the EcoSystems and Chemistry of the Arctic Pacific Environment (ICESCAPE) program. They concluded that RWW presence was an important factor controlling biological productivity on the Chukchi shelf.

SCM and associated subsurface productivity maxima have been the focus of studies in nearly every subregion of the Arctic (e.g., Ardyna et al., 2013; Bouman et al., 2020; Hill & Cota, 2005; Martin et al., 2010). A number of studies focused on the NE Chukchi shelf are of particular relevance to our discussion. Brown et al., (2015) found that SCM depth was strongly positively correlated to euphotic and nitracline depths in early season cruise data (June-July) associated with the ICESCAPE program. Additionally, their analysis of historical CTD data from the Chukchi suggested a gradual deepening of SCM from ~20 m in May (pre-ice retreat) to ~30 m in June, with SCM stabilizing at approximately 30 m through September. They took the latter to be evidence that (1) 30 m is the approximate limit for the euphotic depth in this region; and 2) SCM are actively maintained through summer by upward diffusion of NO_3 from the nitracline. They further argued that colored dissolved organic matter (CDOM) presence in surface waters was an important factor limiting euphotic depth to 30 m on the Chukchi shelf, in contrast to the deeper SCM typically observed off shelf in the Arctic basin. While the Brown et al., (2015) analysis took a shelf-average perspective, Martini et al. (2016) and Weingartner et al. (2017) used high-resolution towed Acrobat surveys of Chl Fl, paired with observations of separately collected discrete nutrients from standard CTD surveys to understand spatial patterns of SCM on the Chukchi shelf. Their analyses pointed toward clear differences in SCM in regions characterized by surface MW, as opposed to those where MW was absent at the surface. Namely, SCM were shallower, thinner, and weaker in the southeast Chukchi where MW was absent and much more robust in the northeast Chukchi where MW was present. They observed significantly higher nitrate concentrations in bottom water underlying MW then in bottom waters associated with SW at the surface, and hypothesized these spatial patterns in bottom water nutrients contributed to SCM patterns (Martini et al., 2016). Weingartner et al., (2017) further noted that MW presence was associated with 2-5x higher density variance over submesoscale ($>$ 5 km) and mesoscale (5-20 km) intervals. They suggested that the higher variance may reflect instabilities associated with fronts (i.e., MW/SW) as well as spatial variations in melt that could contribute to SCM patchiness in the MW hydrographic regime.

4.3 A conceptual model of short-term and long-term control of O_2 and SCM

Our high-resolution observations add additional rich detail and, together with past studies, contribute to a developing understanding of spatial patterns in

SCM and subsurface productivity as inferred from O_2 excess and DIN drawdown. Here, we merge these perspectives into a conceptual model that considers how circulation, mixing, stratification, and light cause surface and subsurface layers of the water column to seasonally evolve in this region (**Figure 9**).

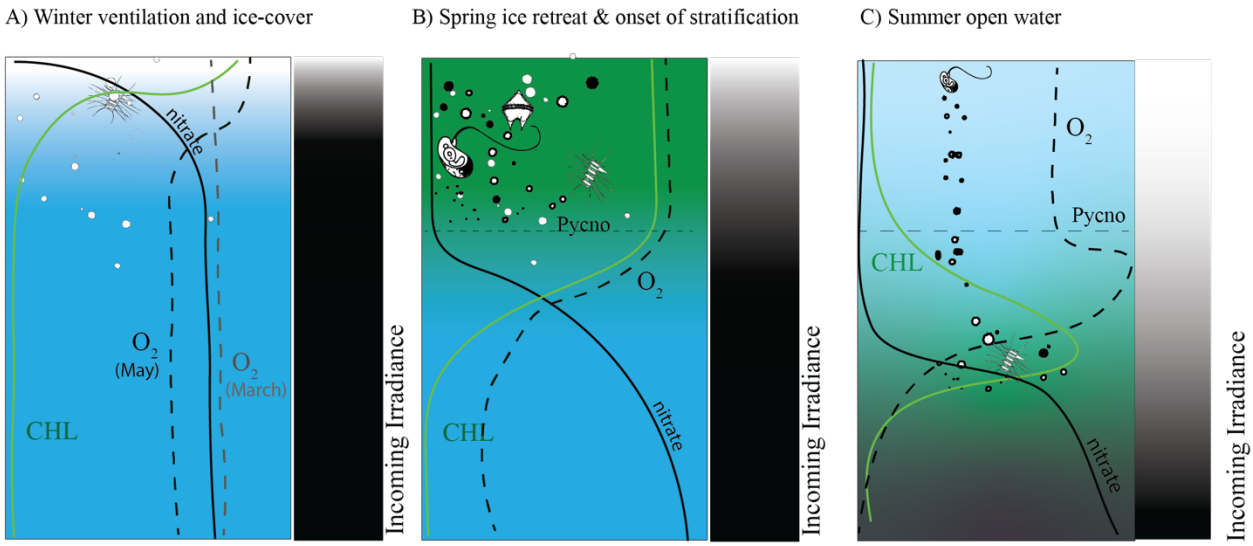

Figure 9: Conceptual diagram of seasonal changes in DIN, Chl, and O_2 as described in the text. Also shown is changing light penetration in the water column as a function of seasonal ice cover or biomass.. Green shading is meant to indicate increased concentration of phytoplankton and/or detrital biomass. Seasonally changing plankton composition is also indicated.

In fall and winter, convective mixing over shallow shelves in the region lead to the formation of low temperature, relatively high salinity water known as newly ventilated winter water (NVWW, Pacini et al., 2019; Pickart et al., 2016). The convective overturn redistributes inorganic nutrients accumulated in bottom water during the previous season over the entire water column while interaction with the atmosphere allows the water column to be ventilated with O_2. The NVWW is advected northward / eastward along major circulation pathways in the Chukchi (**Figure 1**) and additional intermittent mixing in sea ice leads and/or polynyas ensures additional convective mixing and redistribution of nutrients throughout the water column (Pacini et al., 2019; Weingartner et al., 1998). While saturations of O_2 in NVWW have not explicitly been studied, we might expect that ventilation during winter leads to O_2 concentrations within a few percent of equilibrium (O_2 =0%). Cooling of surface water, inherent to NVWW formation (Pacini et al., 2019) would likely result in slightly undersaturated conditions because of the several week timescale needed for the ocean to achieve O_2 equilibrium with the atmosphere, and the potential intermittent

ventilation in patchy sea ice cover in fall and early winter. In contrast, exclusion of gases from the ice matrix during sea ice formation may enhance gas saturations (Top et al., 1985, 1988). Our analysis of Ar saturations (Ar , defined similarly as in eq. 1 but for Ar) in near-bottom RWW in 2016 and 2017 fall into the range of -2% to -5% (data not shown) suggesting that water column O_2 saturations also start out slightly undersaturated due to winter cooling.

This winter water advects northward and eastward through our study area along several key circulation paths before draining off the shelf and into the Arctic deep basin north of Herald Canyon or via Barrow Canyon (**Figure 1**)(Pickart et al., 2016). During transit, NVWW can be slightly modified, resulting in the derivative water mass RWW (Lin et al., 2019; Pickart et al., 2016). The average transit timescale of winter water on the Chukchi shelf depends greatly on the pathway taken through the Chukchi. The Alaskan Coastal Current is the most expedient path at a typical transit timescale of 3 months from Bering Strait to Barrow Canyon while the slowest pathway (~ 6 months) funnels through Herald canyon and then turns eastward and circulates around Hanna Shoal before draining into Barrow Canyon (**Figure 1**, Lin et al., 2019; Shroyer & Pickart, 2018). An intermediate timescale pathway funnels through Central Channel and then turns eastward (**Figure 1**). Consequently, RWW is more likely to be encountered in the northeastern sector of the shelf later in the open water season (Lin et al., 2019; Shroyer & Pickart, 2018).

By early spring, just prior to sea ice retreat, the formation of winter water and its subsequent advection along circulatory pathways primes the system with the nutrient inventory for spring and summer growth. As reported by (Mordy et al., 2020), the regeneration of nutrients in winter is interannually variable, but several years of moored, sensor-based nitrate observations in Chukchi bottom waters indicate a steady increase in bottom water concentrations from winter through early spring, with values typically peaking at 10-15 µmol kg^{-1} by May. These fixed-point time-series observations likely reflect a combination of local and remote processes: the advection of high nutrient NVWW from Bering Strait as well as some subsequent additions of inorganic N as organic matter produced in the previous season is respired (Mordy et al., 2020). This respiration of organic matter in winter/spring under partial or complete ice-cover would drive a proportional undersaturation of O_2.

As sea ice retreats, the water column develops strong stratification from a combination of thermal and haline (meltwater) forcing and the surface layer and mid-depth/lower layers quickly diverge in their physical and biogeochemical character. The nutrient inventory that was contained in the upper, light-replete layer is quickly consumed by phytoplankton growth (Lowry et al., 2015). Below the pycnocline, nutrient-replete waters receive less light, particularly in regions where there is high biomass in the surface from ice-retreat blooms (Ardyna & Arrigo, 2020; Codispoti et al., 2005; Hill et al., 2013). However, as the upper water column becomes oligotrophic and biomass decreases (allowing more light penetration to mid-water column), subsurface productivity in the vicinity of the

nitracline must increasingly dominate integrated water column totals (Ardyna et al., 2013; Ardyna & Arrigo, 2020; Hill et al., 2013). Unlike at the surface, the O_2 produced via net production in mid-depth waters cannot exchange with the atmosphere and therefore accumulates over the course of the season (**Figure 9**).

Following this logic, a ~20 m surface mixed layer replenished with ~10-15 µmol kg^{-1} DIN inventory in winter (Arrigo et al., 2017; Mordy et al., 2020) would have the same net productivity as a 20 m mid-depth layer that also consumes 10-15 µmol kg^{-1} of inorganic N, as seen in portions of the eastern surveys (BC, BHS, **Figure 2**). It is notable that the implied mid-depth DIN demand calculated from accumulated O_2 (5 to 8 µmol kg^{-1} for BC and BHS) represents a substantial fraction of the DIN typically associated with RWW (10-15 µmol kg^{-1}. The discrepancy between the N demand implied from O_2 and the 10-15 µmol kg^{-1} typically observed in RWW could be explained by three scenarios: (1) some fraction of DIN uptake and O_2 generation occurred before stratification onset, with a portion of O_2 produced lost to the atmosphere; (2) some accumulation of the mid-depth O_2 maximum was partially offset by turbulent dispersion over the water column; and (3) O_2 saturations at the start of the season are undersaturated by both physical (2-5% as inferred from deep Ar saturation data) and biological processes (respiration of organic matter in winter/spring), and not equilibrium, as assumed in the simple stoichiometric conversions above. In all cases, the net O_2 accumulation observed in late summer, calculated relative to equilibrium, would indicate a lower bound estimate.

It is of interest that Chl Fl and O_2 maxima are often vertically offset, and the intensity of the two features do not seem to directly correspond. This decoupling is likely a consequence of the very different timescales associated with these biogeochemical tracers. Chl Fl, and the biomass it represents, is likely controlled by shorter timescale processes – an immediate balance between growth supported by nutrient supply rate and loss from sinking, mortality and turbulent dispersion at a given depth horizon. These factors likely work somewhat in opposition to each other, such that higher turbulent nutrient supply rates imply more dispersion of biomass associated with SCM. In this region turbulence varies over short time-and length- scales, in response to surface forcing and subsequent internal instabilities (Beaird et al., 2020; Nishino et al., 2015; Rainville & Woodgate, 2009), which likely contributes to the observed spatial patchiness of Chl Fl. During subsequent time-periods of lower turbulence, the biological response to recent nutrient supply may be evident in higher Chl Fl. However, our observations of coupled Chl Fl and turbulence reveal that in the mean, strong SCM are most frequently associated with water column turbulence minima (**Figure 6**) and bottom water nutrient concentration may be of second order importance (for the range of bottom water DIN seen in our transects). This finding is somewhat in contrast to conclusions derived from prior models of idealized subsurface biomass features, which find that the magnitude of subsurface biomass is strongly controlled by bottom water nutrient concentration (Beckmann & Hense, 2007; Cullen, 2015). Similar upward diffusive nutrient flux

rates despite very different DIN concentration profiles may help to explain why SCM patchiness and intensity were not as clearly aligned with bottom water DIN. While MW presence at the surface seems to contribute to more robust SCM (c.f. BC transect, **Figures 2 & 6**), strong subsurface minima were also encountered when SW was present at the surface and there was a water column turbulence minimum (c.f. WT transects, **Figures 3 & 6**).

In contrast, the processes that control O_2 are dominated by longer, seasonal timescales – the winter replenishment of nutrients throughout the water column, and the inventory of these nutrients that resides within waters with sufficient light, allowing consumption of N and production of O_2. Largest O_2 maxima were encountered overlying high-nutrient RWW, which was frequently associated with MW at the surface (**Figures 4 & 5**). More modest O_2 maxima were encountered in areas where RWW was absent and lower nutrient SW was encountered at the bottom. Shorter time-scale processes may slightly modify the patterns arising from water column nutrient distributions, with turbulent diffusion acting to mix higher O_2 waters to depth while at the same time supplying an upward flux of nutrients to fuel additional photosynthetic O_2 production.

Of course, light must also be sufficient to allow necessary photosynthetic energy production to support metabolism. Surface PAR data ranged from 100 to >2000 µE m^{-2} s^{-1} during our study (e.g., **Figure 8**), with daily integrated PAR ranging from 3 to 60 mol quanta m^{-2} d^{-1} (mean 26.5 ± 15 mol quanta m^{-2} d^{-1}). At the 1% light level this translates to an average photon flux of 0.265 ± .015 mol quanta m^{-2} d^{-1}, the upper end of the range comparable to the light flux that maintains the deep subsurface chlorophyll maximum in the lower latitude Hawaii Ocean time-series Station ALOHA in the North Pacific Ocean (0.415 mol quanta m^{-2} d^{-1}; Letelier et al., 2004). Our analysis of PAR profiles suggests that light attenuation in the turbid lower layer is an important control on SCM depths (**Figure 8**). This turbidity layer and the depth that it is encountered is a function of the water bottom depth, average particle size, and the velocity/shear of the bottom layer. SCM can occur as deep as 40-50 m if the bottom turbidity layer occurs deeper than this horizon (e.g., BC transect, **Figure 2 & 8**). Hence, both surface water clarity and bottom water clarity play an important role in determining SCM depth on the Chukchi shelf. These findings are somewhat in contrast to the hypothesis of Brown et al (2015), who suggested that 30 m marks a light threshold for SCM depth in this region, influenced primarily by attenuation in the surface by CDOM.

4.4 Spatial patterns in O_2 maxima, nitracline, and SCM depth

Given that subsurface O_2 is seasonally accumulated, and we observe clear spatial patterns in O_2 magnitude and extent throughout the study region, an obvious question is: what controls these patterns? As previously discussed, largest O_2 maxima directly overlie areas of high inorganic N concentration (**Figures 2 & 3**) and in T-S space are most frequently associated with RWW (**Figures 4 & 5**) or cold, dense classes of SW (**Figure 7**). The association of RWW and O_2 implicates winter nutrient inventory renewal as a first order process

controlling subsurface productivity potential for the ice-free season, consistent with prior findings linking RWW presence with short-term biological activity (as constrained by Chl Fl; Lowry et al., 2015). Here, O_2 provides a quantitative tracer of cumulative productivity since the onset of stratification, and reveals a clear, extensive association of subsurface production potential with bottom water nutrient concentrations.

As previously discussed, multiple circulation limbs advect RWW through the NE Chukchi shelf (**Figure 1**) with different associated timescales, and hence, in late summer RWW is more likely to be encountered in areas of the northeastern Chukchi serviced by longer circulation pathways. A multi-year (2003-2017) analysis of water mass presence in the NE Chukchi in summer by Lin et al., (2019) found that RWW was concentrated in bottom waters to the north and east of Hanna Shoal in August. Meanwhile, transects further to the west that are primarily influenced by the Alaska Coastal Current and the intermediate, Central Channel pathway (**Figure 1**) are more likely to contain summer origin water masses (i.e., winter water has already been flushed through these regions). These patterns are consistent with our own observations and help to explain the clear contrasts in bottom water nutrients and mid-depth O_2 observed in our 2017 data. The more moderate O_2 found in western transects where RWW was absent and SW dominated are consistent with the overall lower nutrient content of SW. As SW is formed either by modification of RWW or by mixing of Bering shelf water with other water masses of varying nutrient content in the Bering Strait region in summer (Gong & Pickart, 2016) the "time zero" nutrient content of these sections is harder to define. However, mid-depth O_2 evolved (20-40 µmol kg^{-1}) and implied stoichiometric N demand for these transects is consistent with the DIN in bottom waters (~6 µmol kg^{-1}).

In addition to bottom water nutrient patterns, we found clear associations of mid-depth O_2 layer thickness with water mass distributions. In the 3-layered MW, SW, RWW system observed in the northeastern Chukchi, a shallower pycnocline associated with the transition between MW and SW widened the vertical gap between the pycnocline and the nitracline, effectively allowing more real estate for O_2 maxima to evolve. In western transects, the pycnocline occurred deeper, often at the depth or only a few meters above the depth of the nitracline, thus limiting the potential for net production below the pycnocline.

Our observations suggest clear spatial variations in nitracline/SCM depth that appear to track the turbidicline (**Figures 4, 5, 8**), likely controlled by spatial interactions of bathymetry and velocity that govern the depth at which high light attenuation is encountered (**Figures 2,3,6**). If velocities and particle loads are largely similar, deeper bathymetry would result in a deeper turbidicline, and hence, the possibility of a deeper SCM (as seen in BC transect); shallower bathymetry would limit the vertical extent of sufficient light.

Additionally, turbulence minima seem to be associated with robust SCM (**Figure 6**). This observation is a bit counterintuitive since the nutrient fluxes arising from turbulence at SCM would support robust growth. However,

turbulence can vary with surface wind-forcing (Rainville et al., 2011; Rainville & Woodgate, 2009), and short-term enhancements in turbulent diffusivity have the potential to stimulate biological activity during subsequent quiescent periods. Prior observations support the notion of short-term enhancements to nutrient supply associated with enhanced turbulence. Nishino et al., (2015) reported increased upward nitrate fluxes and enhanced surface productivity at an observation site in the northern Chukchi following a wind event with speeds >10 m s^{-1}. In results associated with our study, Beaird et al., (2020) showed evidence of enhanced diapycnal nutrient fluxes associated with submesoscale instabilities following a wind-forced upwelling event in our second BC transect in 2017. Goñi et al. (2021) found that the locus of Chl Fl maxima shifted between water masses in repeated CTD transects before and after wind events during cruises in September 2016 and August 2017. These observations all seem to point toward fine-scale control of SCM intensity by processes occurring over short time and space scales, while the larger controls on SCM depth occur over longer space/time scales controlled, by turbidicline and nutricline depth.

4.5 Timing and significance of subsurface production

As previously discussed, the significance of subsurface production toward annual, regional productivity has been the subject of considerable debate. While our observations do not completely constrain annual subsurface production for our study region, we can make a few scaling arguments based upon our observations. Given a ~20m subsurface layer with a 12 µmol kg^{-1} DIN concentration in RWW (Arrigo et al., 2017; Mordy et al., 2020) at the start of the growing season, we would anticipate 19 g C m^{-2} of subsurface net community production from complete consumption of this inventory. This subsurface net community production not surprisingly represents a substantial proportion of the total net community production for the Chukchi as reported by Codispoti et al. (2013) based on total water column nutrient drawdown (10-70 g C m^{-2}). Dividing the net community production by an average f-ratio (new/total production) of 0.2 to 0.3, as in Codispoti et al. (2013), we arrive at an estimated total subsurface primary production of 60-100 g C m^{-2}. This represents 1/3 to ½ of the total annual primary production of 173 g C m^{-2} recently reported by Hill et al. (2018). This fractional contribution is similar to that previously estimated by Hill et al. (2013) based on primary productivity profile data throughout the Arctic marginal seas.

Clearly subsurface production contributes significantly to net community production and, if f-ratios of 0.2-0.3 are appropriate for mid-depth waters, to primary productivity as well. But much of the argument concerning the importance of subsurface productivity centers on whether or not this contribution is missed by satellite remote sensing of ocean color. One theory suggests that overestimation of total water column production during the early season associated with sea ice retreat may compensate for underestimation of subsurface productivity late in the season (Ardyna et al., 2013; Arrigo & van Dijken, 2011). One might further extend this line of reasoning to suggest that if the majority of the sub-

surface production occurs in a short temporal burst following ice retreat and stratification, that satellite remote sensing algorithms partially capture this signal. Our data only establish constraint on the total subsurface accrual of O_2 and consumption of DIN and not the timing. However, some additional lines of evidence point toward sustained subsurface productivity contributions in late summer. Hill et al. (2018) report that 30% of integrated water column primary productivity in August occurs between the 1% and 30% light level in the northern Chukchi. Combining this with their average water column productivity for August (700 mg C m^{-2} d^{-1}) indicates subsurface production rates of 210 mg C m^{-2} d^{-1}. To generate a net O_2 excess of 1000 mmol m^{-2} (**Figure 4**) between mid-June (approximate ice-retreat) and mid-August (when our observations occurred) requires a net integrated production of ~150 mg C m^{-2} d^{-1} over 60 days. Assuming an f-ratio of 0.3 for net/total production implies an integrated primary production of 500 mg C m^{-2} d^{-1}. These scaling calculations indicate that a significant fraction of observed O_2 excess could be explained by measured late summer rates applied to the ~60 days following ice-retreat. Hence, late season contributions toward net water column productivity should not be overlooked in assessing regional net production.

1. **Implications and Future Directions**

Our unique combination of high-resolution biogeochemical and physical observations offers several new insights regarding the fine-scale layered structuring of nutrients, O_2, and SCM, and the short-term and long-term control of these features by stratification, turbulence, light, and seasonal water mass formation. Additionally, our observations suggest subsurface productivity contributes significantly toward new and total production in this region. We find large O_2 excess at mid-depth controlled by seasonal timescale nutrient regeneration as well as the extent to which that nutrient inventory occupies a non-turbid portion of the water column. Strong O_2 maxima were associated with areas of the study region where high nutrient winter-origin water masses were present. We encountered thickest O_2 maxima in areas of the study region where the turbid lower layer occurred deeper, which also largely coincided with deeper bathymetry; such areas effectively had more vertical real estate where light was sufficient for net production, allowing O_2 to accumulate. The stratification regime of the upper water column also influenced the thickness of the subsurface layer: shallower, strong pycnoclines under regions influenced by MW allowed for largest accumulations of O_2 excess whereas regions where MW was absent and SW was present at the surface had deeper pycnoclines, and a compression of the proportion of the water column that resides above the turbid bottom layer. SCM were similarly influenced by the interaction of bathymetry and turbidity, such that they occur deeper when the turbid bottom layer is also encountered deeper. Additionally, we find SCM were strongly associated with depths of turbulence minima.

How do these insights help us to understand the current and future trajectory of productivity in this region and the rest of the Arctic Ocean? The Chukchi

Sea and the rest of the Arctic Ocean are experiencing profound physical system change, and the responses to this change are likely to be varied and regionally-dependent (Ardyna et al., 2013; Carmack & Wassmann, 2006; Juranek, 2022; Wassmann & Reigstad, 2011). Because the Chukchi resides just downstream of a critical Arctic gateway that supplies a significant proportion of the total nutrient supply to the Arctic Basin (Torres-Valdés et al., 2013) it is very sensitive to physical system changes that impact nutrient transport. Observations from moorings in the Bering Strait region suggest significant freshening of water masses, in particular winter water, over the last several decades, with changes that cannot be solely explained by seasonal sea ice melt (Woodgate & Peralta-Ferriz, 2021). As a consequence, winter water has become significantly less dense over time, which may impact seasonal nutrient replenishment in the Chukchi as well as areas of the Central Arctic Ocean downstream (Woodgate & Peralta-Ferriz, 2021). Bottom line, climate-related trends may be impacting the transport and seasonal replenishment of nutrients in the Chukchi in winter, and as suggested in this study and others, the nutrient inventory of winter water masses is important for setting productivity potential in this region and beyond (Codispoti et al., 2013; Randelhoff et al., 2020; Tremblay et al., 2015). Critically, we have shown that subsurface production associated with winter water masses can be a significant proportion of net water column productivity, and yet changes that may be occurring at mid-depth layers are invisible to passive satellite sensors, which only see what is happening in the surface layer. Clearly, the lack of observing potential beyond the surface is a hindrance to understanding how productive Arctic shelves are responding to change.

As climate-related changes continue to impact the hydrography and nutrient availability in Arctic marginal seas, it will be important to understand the implications of these changes for Arctic ecosystems as well as linkages to other biogeochemical cycles. In this respect, the distinction between new and regenerated production (*sensu* Dugdale & Goering, 1967) is important to note as each has different implications for Arctic ecosystems as well as carbon and nitrogen cycling. New production is that associated with new nutrient sources as opposed to recycling of an existing inventory; new production carries a critical biogeochemical distinction because in a budgetary sense, nutrient inputs (along with associated carbon incorporated into biomass by phytoplankton) can be exported from the system by trophic transfer or settling to benthos, whereas primary production sustained by tight internal recycling (continuous reuse via production and breakdown of biomass) cannot. The large increases in primary production over the last two decades as indicated from satellite-based algorithms (Arrigo & van Dijken, 2015; Lewis et al., 2020) reflect contributions from both new and regenerated production. Indeed, a recent, large-scale Arctic Ocean modeling study indicated that nitrogen input from coastal erosion and terrestrial sources is tightly recycled on Arctic shelves, with modeled primary production 8x the N input (meaning that N was recycled 7 times before being exported; Terhaar et al., 2021). Recycled nitrogen does not support net CO_2 uptake from the atmosphere, nor does it support biomass at higher trophic levels. Hence, it is

important to understand changes in both net productivity and total productivity in response to warming-related trends.

Meanwhile, the subsurface production indicated in this study appears to be strongly related to seasonal nutrient replenishment in winter water; this reflects a new nutrient input to the system over an annual cycle. and hence, the potential for total CO_2 sequestration and biomass gain. Indeed, dissolved O_2 inherently tracks net production below the pycnocline by virtue that strong stratification causes the mid-depth region to function as a nearly closed system, and regeneration requires consumption of O_2. The consumption of nutrients at depth and subsequent export to the benthos helps to support rich benthic hotspots observed in this area (Grebmeier et al., 2015) as well as to trap nutrients on the shelf.

Because typical optical depths for passive remote sensing in the Chukchi are shallower than the mid-depth horizons where our observations indicate later season subsurface productivity is occurring, this activity is unlikely to be captured or tracked by surface-focused ocean color observations. This indicates a critical gap in our ability to detect how net production of Arctic ecosystems may be influenced by changing inflow (and possibly changing nutrient delivery) in this important Arctic gateway region. New, active satellite-based sensors (e.g., light detection and ranging, LIDAR) can sense biomass associated with subsurface "scattering layers" (Churnside et al., 2020; Churnside & Marchbanks, 2015; Hill & Zimmerman, 2010) but conversion of biomass to productivity rate requires knowledge of the interrelationships among subsurface chlorophyll, biomass, and productivity. Clearly, application of new observing approaches and tools to understand what lurks beneath the surface will be critical to understanding how the Pacific Arctic region will respond to change.

Data availability statement: All data associated with this analysis are available in public data repositories. Gridded SuperSucker and turbulence data (excluding PAR) are available at https://doi.org/10.18739/A22F7JR7S. Ungridded SuperSucker data (including PAR) are available at https://doi.org/10.18739/A28S4JP6K. Processed CTD and surface PAR data from *R/V Sikuliaq* cruises are available at the R2R repository (SKQ201612S: https://doi.org/10.7284/125953 ; SKQ201712S: https://doi.org/10.7284/128112). Bottle O_2 /Ar data for SKQ201612S and RB1505 are available at https://doi.org/10.18739/A2B56D48W and https://doi.org/10.18739/A2P26Q39Q, respectively.

Acknowlegements: We thank the marine technicians and crew of the *R/V Sikuliaq* for their excellent assistance in the field. This work was supported by NSF award 1504394 to LJ, BH, and MG, NSF award 1734777 to ES and NB, and NSF award 1949593 to LJ and MG. The authors have no real or perceived conflicts of interest pertaining to this work.

References

Ardyna, M., Babin, M., Gosselin, M., Devred, E., Bélanger, S., Matsuoka, A., & Tremblay, J.-É. (2013). Parameterization of vertical chlorophyll

<i>a</i> in the Arctic Ocean: impact of the subsurface chlorophyll maximum on regional, seasonal, and annual primary production estimates. *Biogeosciences*, *10*(6), 4383–4404. https://doi.org/10.5194/bg-10-4383-2013Ardyna, M., & Arrigo, K. R. (2020). Phytoplankton dynamics in a changing Arctic Ocean. *Nature Climate Change*, *10*(10), 892–903. https://doi.org/10.1038/s41558-020-0905-yArdyna, M., Babin, M., Gosselin, M., Devred, E., Rainville, L., & Tremblay, J.-É. (2014). Recent Arctic Ocean sea ice loss triggers novel fall phytoplankton blooms. *Geophysical Research Letters*, *41*(17), 6207–6212. https://doi.org/10.1002/2014GL061047Arrigo, K. R., Perovich, D. K., Pickart, R. S., Brown, Z. W., van Dijken, G. L., Lowry, K. E., et al. (2012). Massive Phytoplankton Blooms Under Arctic Sea Ice. *Science*, *336*(6087), 1408–1408. https://doi.org/10.1126/science.1215065Arrigo, K. R., & van Dijken, G. L. (2011). Secular trends in Arctic Ocean net primary production. *Journal of Geophysical Research*, *116*(C9). https://doi.org/10.1029/2011JC007151Arrigo, K. R., & van Dijken, G. L. (2015). Continued increases in Arctic Ocean primary production. *Progress in Oceanography*, *136*, 60–70. https://doi.org/10.1016/j.pocean.2015.05.002Arrigo, K. R., Mills, M. M., van Dijken, G. L., Lowry, K. E., Pickart, R. S., & Schlitzer, R. (2017). Late Spring Nitrate Distributions Beneath the Ice-Covered Northeastern Chukchi Shelf: Spring Nitrate on the Chukchi Shelf. *Journal of Geophysical Research: Biogeosciences*, *122*(9), 2409–2417. https://doi.org/10.1002/2017JG003881Barnhart, K. R., Miller, C. R., Overeem, I., & Kay, J. E. (2016). Mapping the future expansion of Arctic open water. *Nature Climate Change*, *6*(3), 280–285. https://doi.org/10.1038/nclimate2848Beaird, N. L., Shroyer, E. L., Juranek, L. W., Hales, B., & Goñi, M. A. (2020). Nutrient-Rich Gravity Current Formed by Upwelling in Barrow Canyon: High-Resolution Observations. *Journal of Geophysical Research: Oceans*, *125*(7). https://doi.org/10.1029/2020JC016160Beckmann, A., & Hense, I. (2007). Beneath the surface: Characteristics of oceanic ecosystems under weak mixing conditions – A theoretical investigation. *Progress in Oceanography*, *75*(4), 771–796. https://doi.org/10.1016/j.pocean.2007.09.002Bouman, H. A., Jackson, T., Sathyendranath, S., & Platt, T. (2020). Vertical structure in chlorophyll profiles: influence on primary production in the Arctic Ocean. *Philosophical Transactions of the Royal Society A: Mathematical, Physical and Engineering Sciences*, *378*(2181), 20190351. https://doi.org/10.1098/rsta.2019.0351Brown, Z. W., Lowry, K. E., Palmer, M. A., van Dijken, G. L., Mills, M. M., Pickart, R. S., & Arrigo, K. R. (2015). Characterizing the subsurface chlorophyll a maximum in the Chukchi Sea and Canada Basin. *Deep Sea Research Part II: Topical Studies in Oceanography*, *118*, 88–104. https://doi.org/10.1016/j.dsr2.2015.02.010Cai, W.-J., Chen, L., Chen, B., Gao, Z., Lee, S. H., Chen, J., et al. (2010). Decrease in the CO2 Uptake Capacity in an Ice-Free Arctic Ocean Basin. *Science*, *329*(5991), 556–559. https://doi.org/10.1126/science.1189338Carmack, E., & Wassmann, P. (2006). Food webs and physical–biological coupling on pan-Arctic shelves: Unifying concepts and comprehensive perspectives. *Progress in Oceanography*, *71*(2–4), 446–477. https://doi.org/10.1016/j.pocean.2006.10.004Carmack,

E., Barber, D., Christensen, J., Macdonald, R., Rudels, B., & Sakshaug, E. (2006). Climate variability and physical forcing of the food webs and the carbon budget on panarctic shelves. *Progress in Oceanography*, *71*(2–4), 145–181. https://doi.org/10.1016/j.pocean.2006.10.005Carmack, E. C., Yamamoto-Kawai, M., Haine, T. W. N., Bacon, S., Bluhm, B. A., Lique, C., et al. (2016). Freshwater and its role in the Arctic Marine System: Sources, disposition, storage, export, and physical and biogeochemical consequences in the Arctic and global oceans. *Journal of Geophysical Research: Biogeosciences*, *121*(3), 675–717. https://doi.org/10.1002/2015JG003140Carmack, E. C. (2007). The alpha/beta ocean distinction: A perspective on freshwater fluxes, convection, nutrients and productivity in high-latitude seas. *Deep Sea Research Part II: Topical Studies in Oceanography*, *54*(23–26), 2578–2598. https://doi.org/10.1016/j.dsr2.2007.08.018Churnside, J. H., & Marchbanks, R. D. (2015). Subsurface plankton layers in the Arctic Ocean: PLANKTON LAYERS IN THE ARCTIC. *Geophysical Research Letters*, *42*(12), 4896–4902. https://doi.org/10.1002/2015GL064503Churnside, J. H., Marchbanks, R. D., Vagle, S., Bell, S. W., & Stabeno, P. J. (2020). Stratification, plankton layers, and mixing measured by airborne lidar in the Chukchi and Beaufort seas. *Deep Sea Research Part II: Topical Studies in Oceanography*, *177*, 104742. https://doi.org/10.1016/j.dsr2.2020.104742Coachman, L. K., Aagaard, K., & Tripp, R. B. (1975). *Bering Strait: The Regional Physical Oceanography*. Seattle, USA: University of Washington Press.Codispoti, L. A., & Richards, F. A. (1971). Oxygen supersaturations in the Chukchi and east Siberian Seas. *Deep Sea Research and Oceanographic Abstracts*.Codispoti, L. A., Flagg, C., Kelly, V., & Swift, J. H. (2005). Hydrographic conditions during the 2002 SBI process experiments. *Deep Sea Research Part II: Topical Studies in Oceanography*, *52*(24–26), 3199–3226. https://doi.org/10.1016/j.dsr2.2005.10.007Codispoti, L. A., Kelly, V., Thessen, A., Matrai, P., Suttles, S., Hill, V., et al. (2013). Synthesis of primary production in the Arctic Ocean: III. Nitrate and phosphate based estimates of net community production. *Progress in Oceanography*, *110*, 126–150. https://doi.org/10.1016/j.pocean.2012.11.006Cullen, J. J. (2015). Subsurface Chlorophyll Maximum Layers: Enduring Enigma or Mystery Solved? *Annual Review of Marine Science*, *7*(1), 207–239. https://doi.org/10.1146/annurev-marine-010213-135111Dugdale, R. C., & Goering, J. J. (1967). UPTAKE OF NEW AND REGENERATED FORMS OF NITROGEN IN PRIMARY PRODUCTIVITY1. *Limnology and Oceanography*, *12*(2), 196–206. https://doi.org/10.4319/lo.1967.12.2.0196Else, B. G. T., Galley, R. J., Lansard, B., Barber, D. G., Brown, K., Miller, L. A., et al. (2013). Further observations of a decreasing atmospheric CO $_2$ uptake capacity in the Canada Basin (Arctic Ocean) due to sea ice loss. *Geophysical Research Letters*, *40*(6), 1132–1137. https://doi.org/10.1002/grl.50268Fennel, K., & Boss, E. (2003). Subsurface maxima of phytoplankton and chlorophyll: Steady-state solutions from a simple model. *Limnology and Oceanography*, *48*(4), 1521–1534. https://doi.org/10.4319/lo.2003.48.4.1521Garcia, H. E., & Gordon, L. I. (1992). Oxygen solubility in seawater: Better fitting equations. *Limnology and Oceanography*, *37*(6), 1307–1312.Gong, D., & Pickart, R. S.

(2016). Early summer water mass transformation in the eastern Chukchi Sea. *Deep Sea Research Part II: Topical Studies in Oceanography*, *130*, 43–55. https://doi.org/10.1016/j.dsr2.2016.04.015Goñi, M. A., Juranek, L. W., Sipler, R. E., & Welch, K. A. (2021). Particulate Organic Matter Distributions in the Water Column of the Chukchi Sea During Late Summer. *Journal of Geophysical Research: Oceans*, *126*(9). https://doi.org/10.1029/2021JC017664Grebmeier, J. M., Bluhm, B. A., Cooper, L. W., Danielson, S. L., Arrigo, K. R., Blanchard, A. L., et al. (2015). Ecosystem characteristics and processes facilitating persistent macrobenthic biomass hotspots and associated benthivory in the Pacific Arctic. *Progress in Oceanography*, *136*, 92–114. https://doi.org/10.1016/j.pocean.2015.05.006Grebmeier, J. M., Moore, S. E., Cooper, L. W., & Frey, K. E. (2019). The Distributed Biological Observatory: A change detection array in the Pacific Arctic – An introduction. *Deep Sea Research Part II: Topical Studies in Oceanography*, *162*, 1–7. https://doi.org/10.1016/j.dsr2.2019.05.005Hales, B., Takahashi, T., & van Geen, A. (2004). High-frequency measurement of seawater chemistry: Flow-injection analysis of macronutrients,. *Limnology and Oceanography*, *2*, 91–101.Hales, B., Takahashi, T., & Bandstra, L. (2005). Atmospheric CO $_2$ uptake by a coastal upwelling system: ATMOSPHERIC CO $_2$ UPTAKE BY A COASTAL UPWELLING SYSTEM. *Global Biogeochemical Cycles*, *19*(1). https://doi.org/10.1029/2004GB002295Hales, B., Moum, J. N., Covert, P., & Perlin, A. (2005). Irreversible nitrate fluxes due to turbulent mixing in a coastal upwelling system. *Journal of Geophysical Research-Oceans*, *110*. https://doi.org/10.1029/2004JC002685Hales, B., Karp-Boss, L., Perlin, A., & Wheeler, P. A. (2006). Oxygen production and carbon sequestration in an upwelling coastal margin. *Global Biogeochemical Cycles*, *20*. https://doi.org/10.1029/2005GB002517Hamme, R. C., Nicholson, D. P., Jenkins, W. J., & Emerson, S. R. (2019). Using Noble Gases to Assess the Ocean's Carbon Pumps. *Annual Review of Marine Science*, *11*(1), 75–103. https://doi.org/10.1146/annurev-marine-121916-063604Hill, V., & Cota, G. (2005). Spatial patterns of primary production on the shelf, slope and basin of the Western Arctic in 2002. *Deep Sea Research Part II: Topical Studies in Oceanography*, *52*(24–26), 3344–3354. https://doi.org/10.1016/j.dsr2.2005.10.001Hill, V., Ardyna, M., Lee, S. H., & Varela, D. E. (2018). Decadal trends in phytoplankton production in the Pacific Arctic Region from 1950 to 2012. *Deep Sea Research Part II: Topical Studies in Oceanography*, *152*, 82–94. https://doi.org/10.1016/j.dsr2.2016.12.015Hill, V. J., & Zimmerman, R. C. (2010). Estimates of primary production by remote sensing in the Arctic Ocean: Assessment of accuracy with passive and active sensors. *Deep Sea Research Part I: Oceanographic Research Papers*, *57*(10), 1243–1254. https://doi.org/10.1016/j.dsr.2010.06.011Hill, V. J., Matrai, P. A., Olson, E., Suttles, S., Steele, M., Codispoti, L. A., & Zimmerman, R. C. (2013). Synthesis of integrated primary production in the Arctic Ocean: II. In situ and remotely sensed estimates. *Progress in Oceanography*, *110*, 107–125. https://doi.org/10.1016/j.pocean.2012.11.005Juranek, L., Takahashi, T., Mathis, J., & Pickart, R. (2019). Significant Biologically Mediated CO $_2$

Uptake in the Pacific Arctic During the Late Open Water Season. *Journal of Geophysical Research: Oceans*. https://doi.org/10.1029/2018JC014568Juranek, L. (2022). Changing Biogeochemistry of the Arctic Ocean: Surface Nutrient and CO2 Cycling in a Warming, Melting North. *Oceanography*. https://doi.org/10.5670/oceanog.2022.120Laws, E. A. (1991). Photosynthetic quotients, new production and net community production in the open ocean. *Deep Sea Research Part A. Oceanographic Research Papers*, *38*(1), 143–167. https://doi.org/10.1016/0198-0149(91)90059-OLetelier, R. M., Karl, D. M., Abbott, M. R., & Bidigare, R. R. (2004). Light driven seasonal patterns of chlorophyll and nitrate in the lower euphotic zone of the North Pacific Subtropical Gyre. *Limnology and Oceanography*, *49*(2), 508–519. https://doi.org/10.4319/lo.2004.49.2.0508Lewis, K. M., van Dijken, G. L., & Arrigo, K. R. (2020). Changes in phytoplankton concentration now drive increased Arctic Ocean primary production. *Science*, *369*(6500), 198–202. https://doi.org/10.1126/science.aay8380Lin, P., Pickart, R. S., McRaven, L. T., Arrigo, K. R., Bahr, F., Lowry, K. E., et al. (2019). Water Mass Evolution and Circulation of the Northeastern Chukchi Sea in Summer: Implications for Nutrient Distributions. *Journal of Geophysical Research: Oceans*, *124*(7), 4416–4432. https://doi.org/10.1029/2019JC015185Lowry, K. E., Pickart, R. S., Mills, M. M., Brown, Z. W., van Dijken, G. L., Bates, N. R., & Arrigo, K. R. (2015). The influence of winter water on phytoplankton blooms in the Chukchi Sea. *Deep Sea Research Part II: Topical Studies in Oceanography*, *118*, 53–72. https://doi.org/10.1016/j.dsr2.2015.06.006Martin, J., Tremblay, J., Gagnon, J., Tremblay, G., Lapoussière, A., Jose, C., et al. (2010). Prevalence, structure and properties of subsurface chlorophyll maxima in Canadian Arctic waters. *Marine Ecology Progress Series*, *412*, 69–84. https://doi.org/10.3354/meps08666Martini, K. I., Stabeno, P. J., Ladd, C., Winsor, P., Weingartner, T. J., Mordy, C. W., & Eisner, L. B. (2016). Dependence of subsurface chlorophyll on seasonal water masses in the Chukchi Sea: CHUKCHI SUBSURFACE CHLOROPHYLL. *Journal of Geophysical Research: Oceans*, *121*(3), 1755–1770. https://doi.org/10.1002/2015JC011359Matrai, P. A., Olson, E., Suttles, S., Hill, V., Codispoti, L. A., Light, B., & Steele, M. (2013). Synthesis of primary production in the Arctic Ocean: I. Surface waters, 1954–2007. *Progress in Oceanography*, *110*, 93–106. https://doi.org/10.1016/j.pocean.2012.11.004McLaughlin, F. A., & Carmack, E. C. (2010). Deepening of the nutricline and chlorophyll maximum in the Canada Basin interior, 2003-2009: DEEPENING OF THE CANADA BASIN NUTRICLINE. *Geophysical Research Letters*, *37*(24), n/a-n/a. https://doi.org/10.1029/2010GL045459Mobley, C. D., & Boss, E. S. (2012). Improved irradiances for use in ocean heating, primary production, and photo-oxidation calculations. *Applied Optics, 51*, 6549–6560. https://doi.org/10.1364/AO.51.006549Mordy, C. W., Bell, S., Cokelet, E. D., Ladd, C., Lebon, G., Proctor, P., et al. (2020). Seasonal and interannual variability of nitrate in the eastern Chukchi Sea: Transport and winter replenishment. *Deep Sea Research Part II: Topical Studies in Oceanography*, *177*, 104807. https://doi.org/10.1016/j.dsr2.2020.104807Morel, A., Huot, Y.,

Gentili, B., Werdell, P. J., Hooker, S. B., & Franz, B. A. (2007). Examining the consistency of products derived from various ocean color sensors in open ocean (Case 1) waters in the perspective of a multi-sensor approach. *Remote Sensing of Environment, 111*, 69–88. https://doi.org/10.1016/j.rse.2007.03.012Moum, J. N. (2015). Ocean speed and turbulence measurements using pitot-static tubes on moorings. *Journal of Atmospheric and Oceanic Technology*, *32*(7), 1400–1413.Moum, J. N., & Nash, J. D. (2009). Mixing measurements on an equatorial ocean mooring. *Journal of Atmospheric and Oceanic Technology*, *26*(2), 317–336. https://doi.org/10.1175/2008JTECHO617.1Nishino, S., Kawaguchi, Y., Inoue, J., Hirawake, T., Fujiwara, A., Futsuki, R., et al. (2015). Nutrient supply and biological response to wind-induced mixing, inertial motion, internal waves, and currents in the northern Chukchi Sea. *Journal of Geophysical Research: Oceans*, *120*(3), 1975–1992. https://doi.org/10.1002/2014JC010407Ouyang, Z., Qi, D., Chen, L., Takahashi, T., Zhong, W., DeGrandpre, M. D., et al. (2020). Sea-ice loss amplifies summertime decadal CO2 increase in the western Arctic Ocean. *Nature Climate Change*, *10*(7), 678–684. https://doi.org/10.1038/s41558-020-0784-2Pabi, S., van Dijken, G. L., & Arrigo, K. R. (2008). Primary production in the Arctic Ocean, 1998–2006. *Journal of Geophysical Research*, *113*(C8). https://doi.org/10.1029/2007JC004578Pacini, A., Moore, G. W. K., Pickart, R. S., Nobre, C., Bahr, F., Våge, K., & Arrigo, K. R. (2019). Characteristics and Transformation of Pacific Winter Water on the Chukchi Sea Shelf in Late Spring. *Journal of Geophysical Research: Oceans*, *124*(10), 7153–7177. https://doi.org/10.1029/2019JC015261Petty, A. A., Stroeve, J. C., Holland, P. R., Boisvert, L. N., Bliss, A. C., Kimura, N., & Meier, W. N. (2018). The Arctic sea ice cover of 2016: a year of record-low highs and higher-than-expected lows. *The Cryosphere*, *12*(2), 433–452. https://doi.org/10.5194/tc-12-433-2018Pickart, R. S., Spall, M. A., Moore, G. W. K., Weingartner, T. J., Woodgate, R. A., Aagaard, K., & Shimada, K. (2011). Upwelling in the Alaskan Beaufort Sea: Atmospheric forcing and local versus non-local response. *Progress in Oceanography*, *88*(1–4), 78–100. https://doi.org/10.1016/j.pocean.2010.11.005Pickart, R. S., Schulze, L. M., Moore, G. W. K., Charette, M. A., Arrigo, K. R., van Dijken, G., & Danielson, S. L. (2013). Long-term trends of upwelling and impacts on primary productivity in the Alaskan Beaufort Sea. *Deep Sea Research Part I: Oceanographic Research Papers*, *79*, 106–121. https://doi.org/10.1016/j.dsr.2013.05.003Pickart, R. S., Moore, G. W. K., Mao, C., Bahr, F., Nobre, C., & Weingartner, T. J. (2016). Circulation of winter water on the Chukchi shelf in early Summer. *Deep Sea Research Part II: Topical Studies in Oceanography*, *130*, 56–75. https://doi.org/10.1016/j.dsr2.2016.05.001Pickart, R. S., Nobre, C., Lin, P., Arrigo, K. R., Ashjian, C. J., Berchok, C., et al. (2019). Seasonal to mesoscale variability of water masses and atmospheric conditions in Barrow Canyon, Chukchi Sea. *Deep Sea Research Part II: Topical Studies in Oceanography*, *162*, 32–49. https://doi.org/10.1016/j.dsr2.2019.02.003Rainville, L., & Woodgate, R. A. (2009). Observations of internal wave generation in the seasonally ice-free Arctic. *Geophysical Research Letters*, *36*(23). https://doi.org/10.1029/2009GL041291Rainville, L., Lee, C., & Woodgate,

R. (2011). Impact of Wind-Driven Mixing in the Arctic Ocean. *Oceanography*, *24*(3), 136–145. https://doi.org/10.5670/oceanog.2011.65Randelhoff, A., Holding, J., Janout, M., Sejr, M. K., Babin, M., Tremblay, J.-É., & Alkire, M. B. (2020). Pan-Arctic Ocean Primary Production Constrained by Turbulent Nitrate Fluxes. *Frontiers in Marine Science*, *7*, 150. https://doi.org/10.3389/fmars.2020.00150Rantanen, M., Karpechko, A. Yu., Lipponen, A., Nordling, K., Hyvärinen, O., Ruosteenoja, K., et al. (2022). The Arctic has warmed nearly four times faster than the globe since 1979. *Communications Earth & Environment*, *3*(1), 168. https://doi.org/10.1038/s43247-022-00498-3Redfield, A. C., Ketchum, B. H., & Richards, F. A. (1963). The Influence of Organisms on the Composition of the Sea Water. In M. N. Hill (Ed.), *The Sea* (Vol. 2, pp. 26–77). New York: Interscience Publishers.Sakshaug, E. (2004). Primary and secondary production in the Arctic Seas. In *The organic carbon cycle in the Arctic Ocean* (pp. 57–81). Springer.Shroyer, E. L., & Pickart, R. S. (2018). Pathways, timing, and evolution of Pacific Winter Water through Barrow Canyon. *Deep Sea Research Part II: Topical Studies in Oceanography*. https://doi.org/10.1016/j.dsr2.2018.05.004Stammerjohn, S., Massom, R., Rind, D., & Martinson, D. (2012). Regions of rapid sea ice change: An inter-hemispheric seasonal comparison: REGIONS OF RAPID SEA ICE CHANGE. *Geophysical Research Letters*, *39*(6), n/a-n/a. https://doi.org/10.1029/2012GL050874Stanley, R. H. R., Jenkins, W. J., Lott, D. E., & Doney, S. C. (2009). Noble gas constraints on air-sea gas exchange and bubble fluxes. *Journal of Geophysical Research*, *114*(C11). https://doi.org/10.1029/2009JC005396Stroeve, J., & Notz, D. (2018). Changing state of Arctic sea ice across all seasons. *Environmental Research Letters*, *13*(10), 103001. https://doi.org/10.1088/1748-9326/aade56Sverdrup, H. U. (1953). On Conditions for the Vernal Blooming of Phytoplankton. *ICES Journal of Marine Science*, *18*(3), 287–295. https://doi.org/10.1093/icesjms/18.3.287Terhaar, J., Lauerwald, R., Regnier, P., Gruber, N., & Bopp, L. (2021). Around one third of current Arctic Ocean primary production sustained by rivers and coastal erosion. *Nature Communications*, *12*(1), 169. https://doi.org/10.1038/s41467-020-20470-zTop, Z., Martin, S., & Becker, P. (1985). On the dissolved surface oxygen supersaturation in the Arctic. *Geophysical Research Letters*, *12*(12), 821–823. https://doi.org/10.1029/GL012i012p00821Top, Z., Martin, S., & Becker, P. (1988). A laboratory study of dissolved noble gas anomaly due to ice formation. *Geophysical Research Letters*, *15*(8), 796–799. https://doi.org/10.1029/GL015i008p00796Torres-Valdés, S., Tsubouchi, T., Bacon, S., Naveira-Garabato, A. C., Sanders, R., McLaughlin, F. A., et al. (2013). Export of nutrients from the Arctic Ocean: ARCTIC OCEAN NUTRIENT EXPORTS. *Journal of Geophysical Research: Oceans*, *118*(4), 1625–1644. https://doi.org/10.1002/jgrc.20063Tremblay, J.-É., & Gagnon, J. (2009). The effects of irradiance and nutrient supply on the productivity of Arctic waters: a perspective on climate change. In J. C. J. Nihoul & A. G. Kostianoy (Eds.), *Influence of Climate Change on the Changing Arctic and Sub-Arctic Conditions* (pp. 73–93). Dordrecht: Springer Nether-

lands. https://doi.org/10.1007/978-1-4020-9460-6_7Tremblay, J.-É., Anderson, L. G., Matrai, P., Coupel, P., Bélanger, S., Michel, C., & Reigstad, M. (2015). Global and regional drivers of nutrient supply, primary production and CO2 drawdown in the changing Arctic Ocean. *Progress in Oceanography*, *139*, 171–196. https://doi.org/10.1016/j.pocean.2015.08.009Tu, Z., Le, C., Bai, Y., Jiang, Z., Wu, Y., Ouyang, Z., et al. (2021). Increase in CO $_2$ Uptake Capacity in the Arctic Chukchi Sea During Summer Revealed by Satellite-Based Estimation. *Geophysical Research Letters*, *48*(15). https://doi.org/10.1029/2021GL093844Walsh, J. J., Mcroy, C. P., Coachman, L. K., Goering, J. J., Nihoul, J. J., Whitledge, T. E., et al. (1989). Carbon and nitrogen cycling within the Bering/Chukchi Seas: Source regions for organic matter effecting AOU demands of the Arctic Ocean. *Progress in Oceanography*, *22*, 277–359.Wassmann, P., & Reigstad, M. (2011). Future Arctic Ocean Seasonal Ice Zones and Implications for Pelagic-Benthic Coupling. *Oceanography*, *24*(3), 220–231. https://doi.org/10.5670/oceanog.2011.74Wassmann, P., Krause-Jensen, D., Bluhm, B. A., & Janout, M. (2021). Editorial: Towards a Unifying Pan-Arctic Perspective of the Contemporary and Future Arctic Ocean. *Frontiers in Marine Science*, *8*, 678420. https://doi.org/10.3389/fmars.2021.678420Weingartner, T., Fang, Y.-C., Winsor, P., Dobbins, E., Potter, R., Statscewich, H., et al. (2017). The summer hydrographic structure of the Hanna Shoal region on the northeastern Chukchi Sea shelf: 2011–2013. *Deep Sea Research Part II: Topical Studies in Oceanography*, *144*, 6–20. https://doi.org/10.1016/j.dsr2.2017.08.006Weingartner, T. J., Cavalieri, D. J., Aagaard, K., & Sasaki, Y. (1998). Circulation, dense water formation, and outflow on the northeast Chukchi Shelf. *Journal of Geophysical Research: Oceans*, *103*(C4), 7647–7661. https://doi.org/10.1029/98JC00374Woodgate, R., & Peralta-Ferriz, C. (2021). Warming and Freshening of the Pacific Inflow to the Arctic From 1990-2019 Implying Dramatic Shoaling in Pacific Winter Water Ventilation of the Arctic Water Column. *Geophysical Research Letters*, *48*(9). https://doi.org/10.1029/2021GL092528Yamagami, A., Matsueda, M., & Tanaka, H. L. (2017). Extreme Arctic cyclone in August 2016: Extreme Arctic cyclone in August 2016. *Atmospheric Science Letters*, *18*(7), 307–314. https://doi.org/10.1002/asl.757